J. PREINE (Orcid ID : 0000-0002-4481-2815)

The Hidden Giant: How a rift pulse triggered a cascade of sector collapses and voluminous secondary mass-transport events in the early evolution of Santorini

J. Preine[1*], J. Karstens[2], C. Hübscher[1], G. J. Crutchley[2], T.H. Druitt[3], F. Schmid[2], P. Nomikou[4]

[1]*University of Hamburg, Institute of Geophysics, Bundesstrasse 55, 20146 Hamburg, Germany*

[2]*GEOMAR Helmholtz Centre for Ocean Research Kiel, Wischhofsstrasse 1-3, 24148 Kiel, Germany*

[3]*CNRS, IRD, OPGC, Laboratoire Magmas et Volcans, Université Clermont Auvergne, F-63000 Clermont-Ferrand, France*

[4]*National and Kapodistrian University of Athens, Department of Geology and Geoenvironment, Panepistimioupoli Zografou, 15784 Athens, Greece*

*corresponding author, jonas.preine@uni-hamburg.de, ORCID: 0000-0002-4481-2815

Conflicts of Interest

The authors declare that they have no known competing financial interests or personal relationships that could have appeared to influence the work reported in this paper.

Data availability

The data that support the findings of this study are available from the corresponding author upon reasonable request.

ABSTRACT

Volcanic island sector collapses have the potential to trigger devastating tsunamis and volcanic eruptions that threaten coastal communities and infrastructure. Considered one of the most hazardous volcano-tectonic regions in the world, the Christiana-Santorini-Kolumbo Volcanic Field (CSKVF) lies in the South Aegean Sea in an active rift zone. Previous studies identified an enigmatic voluminous mass-transport deposit west and east of Santorini emplaced during the early evolution of the edifice. However, the distribution and volume as well as the nature and emplacement dynamics of this deposit remained unknown up to now. In this study, we use an extensive dataset of high-resolution seismic profiles to unravel the distribution and internal architecture of this deposit. We show that it is located in all basins surrounding Santorini and has a bulk volume of up to 125 km^3, thus representing the largest known volcanic island mass-transport deposit in the entire Mediterranean Sea. We propose that the deposit is the result of a complex geohazard cascade that was initiated by an intensive rift pulse. This rifting event triggered a series of smaller precursory mass-transport events before large-scale sector collapses occurred on the northeastern flank of the extinct Christiana Volcano and on the southeastern flank of the nascent Santorini. This was followed by the emplacement of large-scale secondary sediment failures on the slopes of Santorini, which transitioned into debris and turbidity flows that traveled far into the neighboring rift basins. Following this cascade, a distinct change in the volcanic behavior of the CSKVF occurred, suggesting a close relationship between crustal extension, mass transport, and volcanism. Cascading geohazards seem to be more common in the evolution of marine volcanic systems than previously appreciated. Wider awareness and a better understanding of cascading effects are crucial for more holistic hazard assessments.

1.   INTRODUCTION

Submarine landslides offshore volcanic islands are among the largest-volume mass movements on Earth's surface (Moore et al., 1994; Masson et al., 2002). Individual landslide deposits can contain hundreds to thousands of cubic kilometers of material extending over distances of hundreds of kilometers (Moore et al., 1989). These collapse events are capable of generating devastating tsunamis on oceanic scales (Løvholt et al., 2008) and the associated unloading of the volcanic systems may trigger explosive volcanic eruptions (Siebert, 1984; Hunt et al., 2018). In

recent years, marine geophysical surveys have revealed that sector collapses around volcanic islands are a common and important process during the evolution of volcanic edifices, and might occur in complex disaster cascades involving volcanic eruptions, tsunamis, and earthquakes (Ida & Voight, 1995; McGuire, 1996; Voight, 2000; Hunt et al., 2018; Karstens et al., 2019; Patrick et al., 2020; Watt et al., 2021). Understanding the origin, preconditions, and triggers of volcanic sector collapses, as well as their emplacement dynamics in the marine realm, is crucial for determining the magnitude of associated tsunamis and their potential influence on local volcanic systems.

Given the complexity of submarine volcanic landslides, many questions remain open regarding potential trigger mechanisms, emplacement dynamics, and the role of secondary failure processes. Recent studies have shown that landslide volumes are often much greater than the volume of the associated sector collapse scars, which implies significant incorporation of seafloor sediment into the mobilized volume (Watt et al., 2012; 2021; Karstens et al., 2019; Kühn et al., 2021). Watt et al. (2012) noted that many submarine landslide deposits from volcanic islands are characterized by a blocky-surfaced proximal part, which mainly comprises collapsed volcanic material, and a smoother-surfaced apron, which mainly comprises seafloor sediment. The entrainment of secondary sediment into volcanic landslides can be very widespread on low (<1°) gradients and may dominate the total landslide volume (Watt et al. 2012; Crutchley et al., 2013). At Ritter Island, for example, only 20% of the total volume that was deformed or mobilized as part of the collapse was derived from the rapid, tsunami-generating volcanic collapse (Karstens et al., 2019; Watt et al., 2019). Further, results from IODP Expedition 340 showed that the distal and medial parts of landslide deposits offshore Montserrat and Martinique lacked coarse and chaotic subaerial volcanic debris avalanche material, but comprised turbidites and hemipelagic deposits derived from secondary sediment failures (Brunet et al., 2016; Le Friant et al., 2015; 2019).

To explain the occurrence of such voluminous secondary sediment failures at volcanic islands, it has been proposed that the rapid emplacement of failed volcanic edifice material initiates the propagation of a décollement, which causes widespread failure of pre-existing low-gradient seafloor sediment (Watt et al. 2012). According to this model, the load imposed by the initial failure may generate excess pore fluid pressure and trigger additional sediment failures in slope

and basin areas that would not otherwise be prone to failure (Viesca and Rice, 2012; Le Friant et al., 2015; 2019). These results have important implications for the magnitude of tsunami generation by volcanic island landslides since secondary seafloor sediment failures are likely to be much less tsunamigenic than the proximal, block-rich, mass flows (Watt et al., 2012; Le Friant et al., 2019). Therefore, the complexities within submarine volcanic landslides must be carefully considered for an accurate assessment of associated hazards (Watt et al., 2021).

Although volcanic sector collapses are fairly common in the evolution of volcanic edifices, systematic surveys of their remnants are only available for a small number of volcanic island groups and arcs (Watt et al., 2021). Examples from the Hellenic Volcanic Arc in the densely populated Aegean Sea are sparse despite the known occurrence of large-scale volcanic centers and enhanced seismicity, which make this arc one of the major risk factors for the eastern Mediterranean (Sørensen et al., 2012). Preine et al. (2022) reported a large mass-transport deposit within the Christiana-Santorini-Kolumbo volcanic field (CSKVF) in the central Aegean Sea. Chrono-stratigraphic relationships indicate that the deposit was emplaced during the early evolution of Santorini, approximately 0.7 Myrs ago (Preine et al., 2022). However, the distribution, volume, trigger mechanisms, and emplacement dynamics of the deposit have not been investigated so far.

Since 2006, we have compiled a comprehensive dataset of more than 3,200 km of high-resolution multi- and single-channel seismic reflection data (Sigurdsson et al., 2006; Hübscher et al., 2006; Karstens et al., 2020) covering the entire basin system adjacent to Santorini (Fig. 1B). Using this extensive dataset, the first objective of this study is to map the distribution of the large mass-transport deposit (MTD) and estimate its volume. Our second objective is to investigate the nature of this deposit and identify kinematic indicators to determine potential sources. The third objective of this study is to reconstruct its emplacement dynamics, analyze cascading effects, assess its impact on the shallow volcanic plumbing system of the CSKVF, and discuss implications for geohazard assessment.

2. GEOLOGICAL FRAMEWORK

The marine CSKVF is one of the most hazardous volcano-tectonic fields in the world (Druitt et al., 1999). It is located on the Hellenic Volcanic Arc, which stretches from Greece in the west towards Turkey in the east and was formed as a consequence of the subduction of the Nubian

underneath the Eurasian Plate (Fig. 1A) (Le Pichon & Angelier, 1981). Having produced over 100 explosive eruptions including at least four caldera collapses during the last 360,000 years, the CSKVF poses a major threat (eruptions, tsunamis, earthquakes) to the eastern Mediterranean region (Druitt et al., 1999; Nomikou et al., 2016a; Kutterolf 2021a; 2021b; Satow et al., 2021). The iconic Minoan Eruption ~3600 years before present may have contributed to the fall of the great Minoan civilization, leaving its imprint on Greek mythology, archeology, and volcanology (Druitt et al., 2019).

Situated on highly stretched continental crust in an SW-NE oriented rift zone, the CSKVF comprises the extinct Christiana Volcano, the Santorini Caldera, the polygenetic submarine Kolumbo Volcano, as well as the Kolumbo Volcanic Chain (Fig. 1B) (Nomikou et al., 2012; 2013; Hübscher et al., 2015; Hooft et al., 2017; 2019; Preine et al., 2022). The CSKVF is located on the junction of the broad Christiana Basin to the West and the complex Santorini-Amorgos Tectonic Zone (SATZ) to the East (Fig. 1B) (Nomikou et al., 2018, 2019). The Christiana Basin has been named after the Christiana Islands, a group of three highly eroded volcanic islets belonging to the same submarine edifice southwest of Santorini (Fig. 1B, 3G), which is assumed to have been dormant since the Early Pleistocene (Preine et al., 2022). There are three larger volcanic domes (200-300 m volcanic relief) east of Christiana, which are partially cut by SW-NE trending faults (Nomikou et al., 2013). As a zone of SW-NE trending rifts, the SATZ extends from the eastern flank of Santorini towards Amorgos and separates the Cycladic Plateau to the northwest from the minor Anafi-Astypalaea Plateau to the southeast (Nomikou et al., 2018, 2019). These complex tectonic horst and graben segments evolved during four major tectonic pulses and are bordered by SW-NE trending active extensional to transtensional faults (Hübscher et al., 2015; Nomikou et al., 2016b; 2018; Hooft et al., 2017; Preine et al., 2020).

Besides the occurrence of pyroclastic-flow deposits from the recent (<0.36 Ma) eruptions of Santorini forming the Thera Pyroclastic Formation (Sigurdsson et al., 2006; Hübscher et al., 2015; Preine et al., 2022), the literature of major MTDs from the basins surrounding the centers of the CSKVF is surprisingly sparse given the long history of volcanic build-up, caldera-collapse and enhanced tectonic exposure (Bohnhoff et al., 2006; Nomikou et al., 2018; Preine et al., 2020). Bell et al. (2013) reported a surficial landslide deposit on the southeastern flank of Santorini, which contained large remobilized blocks composed of pyroclastic-flow deposits from the

Minoan eruption. These authors proposed that this deposit is the result of a landslide that was triggered by a large seismic event after the Minoan eruption (Bell et al., 2013). Tsampouraki-Kraounaki and Sakellariou (2018) reported several chaotic seismic units in the Christiana Basin, including a particularly thick (> 100 ms two-way traveltime (TWT)), transparent unit, which thickens towards Santorini and was interpreted to be of pyroclastic origin that might have been related to an eruption in the early phase of the evolution of Santorini. In a recent study, however, it was shown that this deposit also occurs in the Anhydros Basin on the eastern side of Santorini and that the internal architecture is also consistent with that of a large MTD (Preine et al., 2022). This deposit was emplaced after volcanism aligned southwest and northeast of Santorini, but before the emergence of enhanced, rift-wide volcanism (~0.7 – 0.36 Ma) and the onset of the explosive Thera Pyroclastic Formation (< 0.36 Ma; Preine et al., 2022).

3. GEOPHYSICAL METHODS

In this study, we use a dataset of over 3,200 km of high-resolution multi- and single-channel seismic data collected during several cruises between 2006 and 2019 (Fig. 1B) (Sigurdsson et al., 2006; Hübscher et al., 2006; Karstens et al., 2020). See Appendix A for details regarding the acquisition and processing of the seismic data. All processed seismic lines were combined into an interpretation project using the KingdomSuite software. Here, we established the stratigraphic framework (following the nomenclature in Preine et al., 2022), mapped the seismic unit corresponding to the inferred MTD (Unit 4), and created isopach maps by interpolating between the seismic profiles. Ocean-bottom seismometer recordings and ray-tracing analysis provided seismic velocities (Preine et al., 2022), which we then used to approximate deposit volumes. We estimated the volume of Unit 4 using an interval velocity of 1900 m/s with an uncertainty of ± 100 m/s, which accounts for errors in picking seismic reflections for the applied velocity model and the fact that the interval velocity of Unit 4 was only available at one location (Preine et al., 2022).

4. RESULTS

The stratigraphy of the basins hosting the CSKVF comprises six units (U1-U6), which are separated by six marker horizons h1-h6 at the corresponding base of each unit (following the nomenclature of Preine et al., 2022). In the following, we will focus on the uppermost Units 3-6, with the potential MTD previously defined as Unit 4 (Preine et al., 2022). Figure 2 gives an

overview of the seismic facies within these units (based on concepts of Mitchum et al., 1977). The internal architecture of Unit 3 and Unit 5 consists of a sequence of well-stratified reflections with generally low amplitudes that contrast with the complex architecture of Unit 4 and Unit 6. Within Unit 4 we identify four different seismic subunits (U4a-d) across our working area, highlighting the complex nature of this deposit. At the base of Unit 4, we find a sequence of subparallel to irregular high-amplitude reflections (U4a) at most locations. Only in the vicinity of Santorini, this unit is missing and we identify instead a sequence of deformed, chaotic reflections with moderate amplitudes that are occasionally interrupted by some partially layered reflection sequences (U4b). The largest part of Unit 4 is made up of incoherent strata with transparent seismic facies and some reflection patches of moderate to high amplitudes (U4c). The top of this deposit is marked by wavy reflections with moderate amplitude. Further, we identify a subunit with subparallel to incoherent low-amplitude reflections (U4d). The boundary between each of these identified internal subunits is not always distinct and individual subunits might transition into each other. The uppermost Unit 6 comprises subparallel reflections that are partially interrupted and intercalated with high-amplitude irregular reflections.

4.1 CHRISTIANA BASIN

Figure 3A shows a seismic profile extending from the western flank of Santorini into the Christiana Basin to the west. Unit 3 has an approximately constant thickness while Unit 4 (orange in Fig. 3A) thickens significantly towards the lower slope of Santorini and is characterized by a complex internal seismic architecture. In the upper part of Unit 4, we identify wavy seismic reflections (U4c; Fig. 2), which become weakly reflective but stratified towards the west (U4d; Fig. 2, 3A). Further, there is a characteristic sequence of one to three internal high-amplitude reflections in the lower portion of the deposit (U4a; Fig. 2), with the uppermost of these reflections showing an undulating topography and onlapping the top of Unit 3 (Horizon h4) (Fig. 3A). Unit 4 is overlain by a sequence of closely spaced, well-stratified reflections of Unit 5, which is in turn overlain by Unit 6 (blue in Fig. 3A) that represents the volcanic deposits of the Thera Pyroclastic Formation according to Preine et al. (2022).

Figure 3B shows a seismic line that crosses the Christiana Edifice coming from the west and continues towards the flank of Santorini. West of Christiana, Unit 4 has the same characteristics as observed in Figure 3A: a generally smooth base reflection, a sequence of wavy top-reflections

(U4c; Fig. 2), and a pronounced internal reflection (U4a; Fig. 2, 3B, 3E). Towards Christiana, this internal reflection disappears abruptly at approximately 3 km along the profile, and the distinct base reflection (h4) is interrupted in a region, where the reflections of the underlying Unit 3 are eroded (broken red line west of Christiana in Fig. 3B). The Christiana Edifice is incised by the Christiana Fault scar, forming a distinct step, which is highlighted by the 3D-view in Figure 3G. While the slope of the edifice is smooth towards the west, it is more irregular towards the east. The edifice is covered by a thin, prograding sediment cover (~7.5-8.5 km along profile, Fig. 3B), while the down-faulted hangingwall of the Christiana Fault is overlain by a chaotic sedimentary cover belonging to Unit 5 and 6 (Fig. 3B). Further towards the northeast of Christiana, the slope of the edifice is onlapped by Unit 4, which has a much more complex internal architecture (strongly folded internal reflections, U4b, Fig. 2) here compared to the region northwest of Christiana (Fig. 3B). This deformed sequence of Unit 4 is buttressed against an irregular up-bending structure at the foot of Santorini (Fig. 3B). In addition, we observe that the base of Unit 4 is disrupted here (red dotted line) and that there is pronounced internal folding (Fig. 3F). We also identify a sequence of weak, stratified reflections (U4d; Fig. 2) on top of Unit 4 (Fig 3B).

Figure 3C shows a seismic line crossing the Christiana Fault in NW-SE direction between Christiana and Santorini and ending above one of three larger volcanic domes between Christiana and Santorini. Northwest of the Christiana Fault, Unit 4 is thin (<100 ms) and is interspersed with chaotic high-amplitude reflections. The unit gradually thickens towards the Christiana Fault and then becomes much thicker to the southeast of the fault, exceeding 200 ms thickness in places (e.g. around 10 km along profile). Here, we identify a weak and disrupted base reflection and folding of the internal fabric (U4b; Fig. 2). Towards the southeast, Unit 4 terminates abruptly against the volcanic dome. Again, we identify weakly reflective subunits within the upper part of Unit 4 (U4d; Fig. 2, 3C).

4.2 WESTERN SANTORINI-ANAFI BASIN

The Santorini-Anafi Basin extends from the southeastern flank of Santorini towards the northeast (Fig. 1B). Figure 4A shows a seismic profile that crosses the basin oblique to its rift axis. The upper part of Unit 4 is characterized by transparent seismic facies with some high-amplitude reflection patches (U4c, Fig. 2), while the lower part manifests itself as a sequence of high-amplitude reflections that lap onto the Anafi Fault (U4a, Fig.2). The chaotic upper part thickens

towards the Anafi Fault reaching a maximum thickness of ~100 ms TWT and comprises a sequence of high-amplitude reflection patches. Unit 4 is interbedded between the generally well-stratified reflections of Units 3 and 5, which become less laterally coherent towards the Anafi Fault, where they eventually lose most of their coherency.

On the eastern to the southeastern flank of Santorini, Unit 4 is not continuous but forms three separate depo-centers each separated from each other by prominent normal faults (Fig. 4B). Here, Unit 4 comprises transparent seismic facies interrupted by some high-amplitude, partially layered reflections (U4b, Fig. 2). Between the three depo-centers, Unit 5 lies directly on top of Unit 3 with an erosive unconformity separating both units (Fig. 4D). Several internal reflections within the northernmost depo-center are visible but show an irregular topography, and several irregular positive structures are located at the top of the deposit (U4b, Fig. 2). The southernmost depo-center is fairly thick (up to 150 ms TWT in places) and is also characterized by a distinct hummocky topography, which is draped by the overlying reflections of Unit 5 (Fig. 4D). This irregular blocky topography (Fig. 4E) of the deposit contrasts with the rather smooth appearance is observed at the western Santorini-Anafi Basin (Fig. 4A).

4.3 WESTERN ANHYDROS BASIN

The Anhydros Basin northeast of Santorini hosts the Kolumbo Volcano and the Kolumbo Volcanic Chain (Fig. 1B). As in the previously described basins, we identify a thick, chaotic Unit 4, which is interbedded between Units 3 and 5. Figure 5A shows a seismic profile perpendicular to the basin axis terminating on the northwestern flank of the Kolumbo Volcano, while the profile in 4B crosses the Anhydros Basin in an SW-NE direction. Both profiles show the previously described Unit 4 and numerous faults including the Ios Fault and Kolumbo Fault. While the Ios Fault is a steep marginal fault, the Kolumbo Fault shows a more complex deformation pattern with at least two auxiliary faults. Unit 4 has a generally chaotic and weakly reflective appearance, with a pronounced internal reflection and a smooth base (Fig. 5A, B). In the upper part of the deposits, we identify a sequence of low-amplitude, stratified reflections (U4d, Fig. 2, 5A, 5B). Unit 4 terminates on the slope of Kolumbo above the early eruptive Kolumbo-Unit K2 (Hübscher et al., 2015; Preine et al., 2022), where we observe chaotic internal reflections (Fig. 5A). Towards the north, the deposit terminates against the Ios Fault, with just a thin sequence extending

approximately 1 km further towards the northwest (Fig. 5A). Towards the northeast, we identify a stack of internal reflections near the base of Unit 4, which lap onto the Ios Fault (Fig. 5B).

4.4 EASTERN SANTORINI-ANAFI AND ANHYDROS BASINS

Figure 6A shows a seismic profile crossing the eastern Santorini-Anafi and Anhydros Basins. These basins are large graben and half-graben structures with active marginal faults, which have been interpreted by different workers (e.g., Hübscher et al., 2015; Nomikou et al., 2016b; 2018). Our stratigraphic classification can be correlated with that of Nomikou et al. (2018): Units Sab6/Ab6 and Sab5/Ab5 belong to our Unit 6, while units Sab4/Ab4 correspond to our Unit 5. Unit 4 is part of units Ab4 and Sab4. In the framework of Hübscher et al. (2015), unconformity ab-10 corresponds to horizon h6, and ab-7 corresponds to h4.

Figures 6B and C show that Unit 4 thickens significantly toward the marginal faults (the Ios Fault and the Anhydros Fault) while pinching out away from them. In both basins, the upper part of Unit 4 comprises a sequence of low-amplitude, stratified reflections (U4d; Fig. 2), while the lower part contains a sequence of internal reflections (U4a; Fig. 2, 6B, 6C). The internal reflections in both basins onlap the basal reflection surface h4. In both basins, Unit 4 is the unit with the most significant thickness increase towards the marginal faults (Fig. 6D). Within Unit 5 we identify a chaotic deposit (marked 'slump') in the hanging wall of the Santorini-Anafi Fault (highlighted by the yellow line in Fig. 6C).

4.5 DISTRIBUTION AND VOLUME OF UNIT 4

A comparison of the seismic stratigraphy in all analyzed basins allows correlating Units 3 to 5 based on their internal seismic characteristics (Fig. 7). This stratigraphic fit underlines that Unit 4 occurs in all basins at the same stratigraphic position between Unit 5 and Unit 3. The seismic appearance and internal architecture of Unit 4 are broadly similar in all basins, with chaotic and transparent seismic facies (Fig.2) making up most of the deposit and a package of stacked, high-amplitude coherent reflections existing near the base (Fig. 7). The upper part of Unit 4 in the East Santorini-Anafi Basin is less chaotic than it is in the other basins.

Having identified Unit 4 in all three basins adjacent to Santorini, we mapped its top and base throughout the entire working area and calculated its thickness in TWT. The base of the deposit outlines the general shape of the complex horst and graben structures of the SATZ (Fig. 8A). In front of the hanging wall of the Santorini-Anafi Fault in the eastern Santorini-Anafi Basin, the

base of Unit 4 forms a deep depression, while it becomes very shallow towards the slope of Santorini, where the Anhydros Horst forms a distinctive topographic high, extending towards Santorini. With our new seismic data, we are able to define three previously unrecognized faults complementing the fault network from Nomikou et al. (2016b; 2018; 2019) (black lines in Fig. 8). These additional faults trend SW-NE and extend the fault system from the SATZ towards Santorini. In addition, the Christiana Fault on the northeastern flank of Christiana extends further northeast towards Santorini, suggesting an extension of the SATZ fault system even beneath Santorini.

Unit 4 is present in all basins surrounding Santorini and extends far along the rift basins in the northeast and along the Christiana Basin in the west (Fig. 8B). It has mainly been deposited below the slope break of Santorini and filled up depressions formed by the adjacent rift basins (Fig. 8A and 8B). We identify eight specific depo-centers labeled I-VIII in Figure 8B and their locations, extents, volumes, and relations to faults are summarized in Table 1. The entire deposit, including all depo-centers, covers an area of ~1000 km^2 and has a bulk volume of 118 ± 6.5 km^3.

Table 1: Summary of characteristics of specific depo-centers of Unit 4. Volumes estimated by interpolating between seismic lines, subtracting the TWT-depth of the top reflection of Unit 4 (h5) from that of the base reflection (h4) and depth-conversion using an interval velocity of 1900 m/s with an uncertainty of ± 100 m/s. For location of the depo-centers, see Figure 8B.

Depo-center	Location	Approx. Extent [km^2]	Estimated Volume [km^3]	Figures with crossing seismic line	Related fault
I	Christiana Basin; Northwest of Christiana	360	37 ± 2	Fig. 3A, 3B, 3E, 7, 9A	Christiana Fault
II	Christiana Basin; Between Christiana and Santorini	40	9,4 ± 0,5	Fig. 3B, 3C, 3F	Christiana Fault
III	South of Santorini	30	1.7. ± 0.1	Fig. 4B, 4D, 4E	Southern Santorini Fault
IV	East of Santorini; Between Santorini and Anhydros Horst	27	2 ± 0.2	Fig. 4B	Faults east of Santorini
V	Western Anhydros Basin	200	16.5 ± 1	Fig. 5A, 5B, 7	Kolumbo and Ios Faults
VI	Western Santorini-Anafi Basin	144	8 ± 0.5	Fig. 4A, 7, 9B, 10C	Anafi Fault
VII	Eastern Santorini-Anafi Basin	154	17 ± 1	Fig. 6A, 6C, 7, 10B	Anhydros Fault
VIII	Eastern Anhydros Basin	43	3.5 ± 0.2	Fig. 6A, 6B, 10A	Ios Fault

5 DISCUSSION

5.1 NATURE OF UNIT 4

The stratigraphically complex internal architecture of Unit 4 contrasts strongly with that of the well-stratified Units 3 and 5 (Fig. 2), which we interpret as the deposits of predominantly hemipelagic sedimentation (Preine et al., 2022). Generally, the complex chaotic facies and loss of internal stratification within Unit 4 could result from in-situ deformation, e.g., by fluidization without horizontal displacement (e.g., Ogata et al., 2014), or different mechanics of sediment failure and transport. However, the fact that wherever Unit 4 is not present, Unit 5 lies directly on top of Unit 3 without any seismically resolvable intervening sedimentary sequences, indicates deposition within a relatively short time frame and argues against in-situ deformation or fluidization. Therefore, the most likely processes to explain the chaotic nature of Unit 4 are mass failures or large pyroclastic flows (Crutchley et al., 2013; Karstens et al., 2013).

Tsampouraki-Kraounaki and Sakellariou (2018) proposed a pyroclastic origin for Unit 4 in the Christiana Basin since it thickens towards Santorini and there is no distinct scar on the western side of Santorini. The chaotic architecture of Unit 4 shows similarities to the Thera Pyroclastic Formation in some areas (e.g., Fig. 4A, 5A), which would agree with such an interpretation. However, there is no evidence for any major eruption at that time from nearby onshore outcrops on the Cycladic Islands (e.g. Anafi, Ios, Amorgos, or the basement massif on Santorini), which would be expected due to the abundance and significant volume of Unit 4. Moreover, the internal architecture of Unit 4 shows a strong resemblance to the seismic images of volcanic sector collapse deposits off Montserrat (Lebas et al., 2011; Watt et al., 2012), Ritter Island (Karstens et al., 2019; Watt et al., 2019) and Sakar (Kühn et al., 2021), as well as other non-volcanic mass transport deposits (e.g., Bull et al., 2009; 2020; Posamentier et al., 2011). We identify several instances with features typical for large mass failures, e.g. the distinct lateral margins in the Christiana Basin (Fig. 3C) and Anhydros Basin (Fig. 6A), basal erosion and deformation in front of the Christiana edifice (Fig. 3B, F) and southeast of Santorini (Fig. 4B, C). In general, we observe that the internal reflections within Unit 4 are deformed and complex close to Santorini (Fig. 3B, 3C, 3F, 4B, 4D, 4E), while becoming less chaotic and smoother away from Santorini (3A, 4A, 6A-C). This lateral variation is typical for MTDs and reflects the transition from proximal slumps of granular material into more disintegrated, water-saturated, cohesive debris

flows and turbidity currents in the distal domain (e.g., Bull et al., 2009; Watt et al., 2012; 2019; 2021; Smit et al., 2022). This is observed both at the west (Fig. 3A) and to the east (Figs. 4, 5, 6) of Santorini. The fact that Santorini is surrounded by the proximal facies and the fact that Unit 4 is present in all basins surrounding Santorini implies a transport emanating predominantly from present-day Santorini.

5.2 EMPLACEMENT DYNAMICS

5.2.1 High energy emplacement

In the following, we examine different parts of Unit 4 to find indicators for an erosive, high-energy emplacement to determine potential sources of Unit 4. In the Christiana Basin, our seismic data reveal highly deformed, folded reflections (U4b, Fig. 2) between Christiana and Santorini (Fig. 3A-C) and we observe that parts of Unit 4 are buttressed against an up-bending structure (Fig. 3C), which indicates that Unit 4 is frontally confined in this area (Frey-Martínez et al., 2006). The truncation of underlying reflections (e.g. 'Disrupted Base' in Fig. 3B, C, F), as well as the internal folding within depo-center II (Fig. 8B), imply an erosive emplacement here, whereby the overlying mass transport material scoured into the underlying substrate during transport (Fig. 3B, C). The incised morphology of the Christiana Edifice with a horseshoe-shaped scar is a strong indication for a sector collapse towards the northeast (Fig. 2G). As visible in Figure 3B, the deeper and flatter part of the Christiana scar is directly overlain by Unit 5 and 6, indicating that the formation of the scar corresponds temporally to the emplacement of Unit 4. Consequently, we interpret the folded internal reflections northeast of the Christiana edifice (U4b, Fig. 8B) as the slump deposit from that sector collapse event (Fig. 3B). Such a NE-directed collapse event would explain the abrupt termination of Unit 4 towards the southeast in Figure 3C as being the lateral margin of the collapse deposit. This interpretation is also supported by a comparison of the calculated volume of the deformed strata in front of the Christiana scarp (~4.9 km^3, Fig. 3B, C, F) and the missing volume of the northeast flank of Christiana, which we approximate to be roughly 4.5-5 km^3 from interpolating the missing volume from the bathymetric and seismic data.

We also identify indications for high-energy, erosive emplacement of Unit 4 at the southeastern slope of Santorini (Fig. 4B, depo-centers III and IV in Fig. 8B). Here, Unit 4 is made up mostly of subunit U4b (Fig. 2), with a characteristic blocky topography (Fig. 4B). Such blocky deposits are

commonly considered to be translated blocks (Bull et al., 2009), which have been widely identified around volcanic islands where they are the result of high-energy slumping and are generally restricted to proximal areas of a mass failure event tending to stop at the slope break (Watt et al., 2012; 2019; 2021; Le Friant et al., 2004; 2019). Therefore, we interpret this depo-center as the result of slumping from the southeastern flank of proto-Santorini, which might be associated with activity of the Southern Santorini Fault (Fig. 8B). The nearby coast of present-day Santorini is characterized by the outcrop of the pre-volcanic metamorphic basement, which forms the highest elevation of Santorini at Profitis Ilias (Fig. 4C). Bell et al. (2013) noted a distinct horseshoe-shaped structure on the north-eastern side of Profitis Ilias and several large blocks with crustal lithologies located close to the southeastern coast of Santorini. These blocks have been suspected to be the result of large landslide events, which seems to be an old event that is not related to the surficial landslide deposit observed on the seafloor southeast of Santorini (Bell et al. 2013). Whether a large landslide event from this area has contributed to the emplacement of Unit 4, cannot be determined from the seismic data. It is, however, noteworthy that we only observe the distinct blocky nature of Unit 4 on the southeastern flank of Santorini and nowhere else around Santorini.

5.2.2 Low energy emplacement

The most voluminous parts of Unit 4 are constituted by depo-centers I, V, VI, VII, and VIII, which lie further away from Santorini than depo-centers II-IV (Fig. 8B) and comprise the largely transparent subunit U4c (Fig. 2), the weakly reflective subunit U4d (Fig. 2), the subparallel internal reflections of U4a (Fig. 2) as well as a smooth and laterally continuous base reflection. In contrast to the weak, disrupted and erosional base of Unit 4 observed closer to Santorini (Fig. 3B, 3C, 3F, 4B), the smooth and continuous base implies a lack of basal erosion associated with lower energy emplacement (Watt et al., 2012). The architecture of Unit 4 in these more distal, smoother-shaped deposits fits the definition of frontally emergent MTDs (Frey-Martinez et al. 2006). Such frontally emergent MTDs translate downslope by overthrusting the undisturbed strata and might travel freely over the undeformed slope, evolving into debris and turbidity flows (Frey-Martinez et al. 2006). This mechanism would be in agreement with the internal architecture of Unit 4 in the Christiana Basin (as observed in Fig. 3A), but also with the internal architecture of Unit 4 in the Anhydros and Anafi Basins (Fig. 4A, 5A, 5B, 6A), suggesting that the

transparent, chaotic subunit U4c represents debris flow deposits and the weakly reflective, subparallel subunit U4d represents the turbiditic apron of the deposit (Fig. 2).

Further, we interpret the internal reflections at the base of Unit 4 (U4a) as several smaller stacked MTDs that have been deposited before the upper and most voluminous part of Unit 4. These internal reflections occur mostly in areas where the underlying Unit 3 formed depressions (Fig. 8A). Towards the margins of Unit 4, e.g., on the flank of Santorini (Fig. 3A), the internal reflections disappear and onlap the underlying horizon h4 (Fig. 9). As illustrated in Figure 9, we find instances where there are several larger transparent subunits (up to 40 ms TWT thick) in between these internal reflections indicating that these precursory events had considerable volumes. The uppermost internal reflection is phase reversed in some instances (PR in Fig. 9), which implies the transition from high acoustic impedance to low acoustic impedance. As shown in Sawyer et al. (2009), densification in MTDs plays a major role for the seismic appearance of basal reflections. Typically, densification is greatest near the base and declines upwards (Sawyer et al., 2009). This would imply that the phase-reversed reflection in Unit 4 could be explained by the transition from a more compacted lower part of the upper MTD towards a less compacted upper part of the underlying MTD.

Apart from the horseshoe-shaped scars at Christiana (Fig. 3G) and at Profitis Ilias onshore Santorini (Fig. 4C), we did not find other collapse scars sufficiently large to be correlated to the MTDs of the smoother-shaped depo-centers, leaving the sources of these large depo-centers elusive. However, since we find these deposits predominantly in the depressions of the basins surrounding Santorini (Fig. 8A) with no evidence of basal erosion, a transport emanating from Santorini is most plausible. It is also important to recall that the emplacement of Unit 4 was followed by 0.7 Myrs of intensive volcanic activity of the CSKVF including at least four caldera collapse events (Druitt et al., 1999; Preine et al., 2022), which might have obscured even large collapse scars. For example, Nomikou et al. (2016a) show a profile crossing the western caldera rim of Santorini (their Fig. 4), which shows that the flank deposits are overprinted by young tectonic faults and are overlain by the younger deposits of the TPF. This shows well that the morphology of the collapse scars could be either structurally overprinted and/or covered by subsequent volcanoclastic deposits.

An explanation for these voluminous deposits could be widespread secondary sediment failure and entrapment, as observed around many other volcanic islands (e.g., Watt et al. 2012; 2021; Le Friant et al., 2019). Failed seafloor sediments contribute up to two-thirds to the entire slide volume of volcanic debris-avalanche deposits offshore Montserrat (Watt et al., 2012). Indications for erosion related to such secondary sediment failures are visible at the steep slope of Santorini, where we find evidence for substantial erosion on the southeastern slope between the blocky depo-centers of Unit 4 (2 km along profile; Fig. 4B). Overall, our data show only a thin and rather chaotic sedimentary cover on the slopes of Santorini, which belongs to the uppermost more recently deposited Units 5 and 6. As early volcanism around Santorini was initiated before the emplacement of Unit 4 (Preine et al., 2022), the flanks of proto-Santorini likely consisted of poorly consolidated sediments with weak volcanic material. Therefore, widespread sediment failures from the slopes of proto-Santorini could have been the source for the lower-energy and voluminous deposits observed in all basins explaining why there are no distinct scars related to Unit 4. The lower-energy deposits make up by far the largest volume of Unit 4. Assuming collapse volumes ~4.9 km^3 for Christiana and ~2.5 km^3 for the southeastern flank of Santorini implies that more than 90 % of the total volume of Unit 4 may be the result of secondary seafloor failures.

5.3 TRIGGER MECHANISM

Volcanic sector collapses have been identified in all volcanic settings and their trigger mechanisms range from volcanic intrusions and eruptions, gravitational instabilities, extreme precipitation events, sea-level changes, to earthquakes (Watt et al., 2021). Identifying a specific trigger mechanism is often ambiguous for contemporary sector collapses and becomes even more difficult for an event ~0.7 Myrs ago (Preine et al., 2022). The timing of the emplacement of Unit 4 marks the transition from a phase of relative volcanic dormancy to a phase of basin-wide emergence of volcanoes in the CSKVF and thus large-scale volcano-tectonic processes represent the most likely trigger mechanisms for the observed large-scale mass-transport events.

The tectonic evolution of the CSKVF can be subdivided into four phases that culminated in the evolution of the grabens and half-grabens northeast of Santorini, which formed the previously described basins (Heath et al., 2019; Preine et al., 2022). Opening of these basins occurred in multiple episodes of enhanced rift activity, so-called 'tectonic pulses', which describe distinct episodes of hanging-wall rotation from the marginal faults in such a short time that no

seismically resolvable syn-tectonic deposition occurred (Hübscher et al., 2015). The latest of these episodes can be linked to horizon h4 and thus to the emplacement of Unit 4. The structural relationship between reflection h4 and the marginal faults in the Anhydros and Santorini-Anafi Basins is characterized by a pronounced dip of the basal reflection h4 toward the marginal faults, which is the result of hanging wall rotation of the Ios, Anhydros, and Santorini-Anafi Faults (Fig. 9). In the Anhydros Basin and the western Santorini-Anafi Basin, the internal reflections of Unit 4 have a very different dip compared to the base reflection h4, to which these internal reflections lap onto (Fig. 9). This indicates that hanging wall rotation must have occurred before the deposition of Unit 4 and that this Unit filled up a pre-existing accommodation space. These observations combined are indicators that the deposition of Unit 4 was preceded by a rift-pulse in all basins northeast of Santorini, which is in agreement with the temporal framework of rift activity by Hübscher et al. (2015). However, our dataset reveals that tectonic activity during that episode also affected the Christiana Basin and that the southwest-northeast directed fault trend of the rift basins continues underneath present-day Santorini and extends towards Christiana (Fig. 8), which is in agreement with seismic tomography results (Heath et al., 2019). The Christiana Fault is directly connected to the scarp of the Christiana edifice, which implies a tectonic control of the sector collapse (Figs. 3G).

There are no volcanic deposits correlating to that specific period, while we find a strong indication for enhanced tectonic activity in the entire rift system. Even in phases of regular tectonic activity (as today), the rift is capable of producing energetic earthquakes like the 1956 magnitude 7.4 Amorgos earthquake (Brüstle et al., 2014; Nomikou et al., 2018) and strong earthquakes have been associated with slumping at Santorini before (Bell et al., 2013). Therefore, a strong rift pulse appears to be the most plausible trigger mechanism and can explain the observed widespread and multi-source mass failures at Christiana (Fig. 3) and on the flanks of Santorini (Figs. 3A, 4, 5, 6). However, we see no evidence that fault-induced mass-wasting in the rift basins contributed to Unit 4 farther away from Santorini. We expect that remobilized sediments that have been sourced from the steep faults of the rift basins would show irregular external geometry and chaotic internal reflections. We identify such a deposit in the Santorini-Anafi Basin in the overlying Unit 5 (Figs. 6C and 7, labeled 'slump') but not in Unit 4.

5.4 GEOHAZARD CASCADE

The complexity of seismic facies observed within Unit 4 indicates that its emplacement occurred as a complex cascade of different processes. To explain its emplacement, we propose a cascade of five processes: rifting, precursory mass-movements, sector collapses, secondary sediment failures, and debris flow deposition, as illustrated in Figure 11A-E. In the following, we will refer to Unit 4 as the Santorini Mass-Transport Deposit (SMTD).

As discussed in the previous section, there is evidence that a rift pulse preceded and might have triggered the emplacement of the SMTD. Prior to the main volcanic sector collapse events at Christiana and the southeastern flank of Santorini, we argue that this rift pulse triggered several smaller mass movements, which thus explain the basal subunit within Unit 4 (U4a; Fig. 2, 9, 11C). This order of events is particularly evident at the western flank of Christiana (offset km 1-7 in Fig. 3B), where basal erosion of the SMTD is accompanied by the sudden disappearance of the internal reflections, which indicates that the major collapse of the Christiana Edifice occurred after the deposition of the material associated with the internal reflections (Fig. 911).

Following the model of Watt et al. (2012, 2019) and Le Friant et al. (2019), we propose that the sudden loading by the collapse masses (Fig. 11C) might have led to the propagation of a décollement, which then triggered large-scale secondary sediment failures from the slopes of proto-Santorini (Fig. 11E). We speculate that these failures translated to frontally emergent debris flows, which traveled far throughout the basins filling up the depressions created by the preceding rift pulse. In the last phase of this cascade, turbidites were deposited above the chaotic unit, both near Santorini (Fig. 3B, 3C, 5A, 5B) and further away in the basins (Fig. 3A) explaining the low-amplitude, subparallel subunit U4b (Fig. 2) observed at the top of Unit 4 in many instances. Each of these phases may or may not have been accompanied by volcanic eruptions from proto-Santorini; the actual role of any eruptions cannot be clarified without scientific drilling.

For the same reason, it is difficult to estimate the duration in which the SMTD has been emplaced. However, since we neither found seismically resolvable layers between Units 3 and 5 at locations where Unit 4 is absent nor syn-tectonic reflections within Unit 4 in the rift basins, the duration of the entire cascade from the rift pulse to the proposed secondary sediment failures can be approximated by the vertical seismic resolution. Assuming a vertical seismic resolution of approx. 4-8 m within Unit 4 (assuming an interval velocity of 1900 m/s) and an average

sedimentation rate of 10 cm/kyr (Piper and Perissoratis, 2003; Anastasakis and Piper, 2005; Preine et al., 2022), the SMTD could have been emplaced over a time period of approx. 40-80 kyrs. However, there are reasons to assume that the timespan of the SMTD emplacement was shorter. We have shown that the rift pulse preceded the deposition of the initial mass-wasting event and most of the hanging-wall rotation occurred before the emplacement of the initial MTDs (Fig. 10). It seems reasonable to us that the gap between such a significant tectonic event and the emplacement of large mass wasting deposits was smaller than several tens of thousands of years. Moreover, the propagation of a décollement likely occurred rapidly implying a very short time interval between the sector collapses at Christiana and Santorini and the voluminous secondary sediment failures. However, to exactly determine the timing of the SMTD cascade, scientific drilling is needed.

5.5 IMPACT ON THE VOLCANIC EVOLUTION OF THE CSKVF

Previous studies have shown that landslides may be capable of inducing decompression of subsurface magma storage systems and thus alter eruptive behaviors (Manconi et al., 2009; Pinel and Albino, 2013; Hunt et al., 2018). In the context of the evolution of the CSKVF, it is striking that the emplacement of the SMTD occurred at the transition between two distinctly different volcanic phases (Preine et al., 2022). While the volcanic phase prior to the emplacement of the SMTD was characterized by two SW-NE aligned volcanic centers with comparably low activity (Poseidon and Early Kolumbo, K1/K2; Fig. 11A), the eruptive behavior of the CSKVF changed significantly after the SMTD emplacement with the initiation of basin-wide volcanism (Fig. 11F) (Preine et al., 2022). This subsequent phase saw the construction of the Aspronisi cones SW of Santorini, the eruptions of the Akrotiri rhyolitic centers, the Peristeria stratovolcano, and the monogenetic cinder cones of Aktoriri onshore Santorini, a smaller eruptive sequence at Kolumbo as well as the evolution of the Kolumbo Volcanic Chain (Druitt et al., 1999; Preine et al., 2022) (Fig. 11F). The specific influence of the emplacement of the SMTD sequence on this change in the eruptive behavior cannot be clarified based on the seismic data, since the preceding rift pulse probably also played an important role. However, the relative temporal coincidence of the rift pulse, mass wasting, and the change in eruptive behavior underlines how closely volcanism and crustal tectonics are interconnected at the CSKVF.

5.6 IMPLICATIONS FOR GEOHAZARD ASSESSMENT

With a total volume of 118 ± 6.5 km^3, the SMTD represents the largest known MTD in the Aegean Sea and the largest known volcanic mass-transport deposit in the entire Mediterranean Sea (Urgeles and Camerlenghi, 2013). It is, for example, five times larger than the largest submarine landslide detected offshore Mt Etna (Pareschi et al., 2006). Also in the context of non-volcanic submarine landslides in the Mediterranean, the volume of the SMTD represents a very large event (Urgeles and Camerlenghi, 2013). However, given the uncertainties in the timing of the proposed cascade, it is difficult to properly access the geohazards associated with the emplacement of the SMTD. For example, it has been shown that even time gaps of a few minutes between separate stages of failure can greatly reduce tsunami magnitudes (Løvholt et al., 2008).

Disaster cascades are worldwide phenomena at volcanic islands and have only recently gained wider attention (Hutchison et al., 2016; Walter et al., 2019; Patrick et al., 2020; López-Saavedra et al., 2021). Prominent examples have been reported from the Canaries, where multistage retrogressive landslides were the trigger for caldera-forming eruptions (Hunt et al. 2018). The Ritter Island sector collapse of 1888, the largest in historic time, also involved a cascade of slow flank movement leading to catastrophic collapse and eruption (Karstens et al., 2019; Watt et al., 2019). Even very recent eruptions such as the eruption of Anak Krakatau in 2018, which was triggered by an eruption and slow flank movements (Walter et al., 2019), and Kilauea in 2018 (Patrick et al., 2020) are prominent examples of cascading geohazards.

It would be insightful to study volcano-tectonic systems comparable to the CSKVF for evidence of similar large-scale cascading geohazards, e.g. the hazardous Krakatau volcanic system at the Sunda strait or the volcano-tectonic Kagoshima graben at the northern end of the Ryukyu Arc in the East China Sea (Kamata and Kodama, 1999; Harjono et al., 1991). Both are volcanic back-arc systems that lie in an extensional marine setting and comprise large volcanoes and calderas (Harjono et al., 1991; Tatsumi et al., 2018; Priyanto et al., 2021).

While cascading effects are an inherent challenge for modeling and forecasting (Zuccaro et al., 2018), increased awareness and further research are crucial to ensure greater resilience of coastal communities towards such catastrophic events, especially for regions as vulnerable as the Mediterranean (Walter et al., 2019; Patrick et al., 2020; López-Saavedra et al., 2021).

6. CONCLUSIONS

The analysis of an extensive 2D seismic dataset from the Christiana-Santorini-Kolumbo Volcanic Field has allowed us to identify and map the largest volcanic island mass-transport deposit from the Mediterranean Sea, which occurred in the early phase of the evolution of Santorini ~0.7 Myrs ago. Our results show that emplacement of the Santorini Mass-Transport Deposit (SMTD) likely proceeded as a complex multi-stage cascade, which occurred in all basins surrounding Santorini. We identify five processes that might have contributed to the SMTD cascade: rifting, precursory mass-transport events, catastrophic collapses, secondary sediment failures, and debris flow deposition. Our interpretation is that the emplacement of the SMTD was initiated by an intensive rift pulse, which occurred along SW-NE-directed faults extending from the Christiana Volcano in the southwest towards the island of Amorgos in the northeast (Fig. 11A). Smaller precursory mass-transport events took place before catastrophic frontally confined sector collapses occurred at the northeast flank of the Christiana Volcano and on the southeastern flank of proto-Santorini (Fig. 11B). As a consequence, significant secondary sediment failures on the slopes of proto-Santorini were triggered. These secondary sediment failures are frontally emergent and transitioned into debris flows and turbidity flows that transported large amounts of sediment towards the rift basins northeast of Santorini (Fig. 11C). Constituting by far the largest portion of the entire SMTD sequence (> 90 %), these secondary failures are additional evidence for the importance of secondary processes in the emplacement of mass movements around volcanic islands, and they highlight the key role of reflection seismic surveys in providing detailed insights into such dynamics. The emplacement of the SMTD correlates with a transition from a phase of relative volcanic dormancy to a phase of basin-wide emergence of volcanoes, highlighting how closely volcanism, tectonism, and mass-transport can interact in rift-hosted volcanic systems.

processing software and IHS for providing KINGDOM seismic interpretation software. This is Laboratory of Excellence ClerVolc publication 529.

REFERENCES

Anastasakis, G., & Piper, D. J. (2005). Late Neogene evolution of the western South Aegean volcanic arc: sedimentary imprint of volcanicity around Milos. Marine Geology, 215(3-4), 135-158, https://doi.org/10.1016/j.margeo.2004.11.014

Bell, K. L. C., Carey, S. N., Nomikou, P., Sigurdsson, H., & Sakellariou, D. (2013). Submarine evidence of a debris avalanche deposit on the eastern slope of Santorini volcano, Greece. Tectonophysics, 597, 147-160, https://doi.org/10.1016/j.tecto.2012.05.006

Bohnhoff, M., Rische, M., Meier, T., Becker, D., Stavrakakis, G., & Harjes, H. P. (2006). Microseismic activity in the Hellenic Volcanic Arc, Greece, with emphasis on the seismotectonic setting of the Santorini–Amorgos zone. Tectonophysics, 423(1-4), 17-33, https://doi.org/10.1016/j.tecto.2006.03.024

Brunet, M., Le Friant, A., Boudon, G., Lafuerza, S., Talling, P., Hornbach, M., ... & IODP Expedition 340 Science Party. (2016). Composition, geometry, and emplacement dynamics of a large volcanic island landslide offshore M artinique: From volcano flank-collapse to seafloor sediment failure?. Geochemistry, Geophysics, Geosystems, 17(3), 699-724, https://doi.org/10.1002/2015GC006034

Brüstle, A., Friederich, W., Meier, T., & Gross, C. (2014). Focal mechanism and depth of the 1956 Amorgos twin earthquakes from waveform matching of analogue seismograms. Solid Earth, 5(2), 1027-1044, https://doi.org/10.5194/se-5-1027-2014

Bull, S., Cartwright, J., & Huuse, M. (2009). A review of kinematic indicators from mass-transport complexes using 3D seismic data. Marine and Petroleum Geology, 26(7), 1132-1151, https://doi.org/10.1016/j.marpetgeo.2008.09.011

Bull, S., Browne, G. H., Arnot, M. J., & Strachan, L. J. (2020). Influence of mass transport deposit (MTD) surface topography on deep-water deposition: an example from a predominantly fine-grained continental margin, New Zealand. Geological Society, London, Special Publications, 500(1), 147-171, https://doi.org/10.1144/SP500-2019-192

Crutchley, G. J., Karstens, J., Berndt, C., Talling, P. J., Watt, S. F. L., Vardy, M. E., ... & Maeno, F. (2013). Insights into the emplacement dynamics of volcanic landslides from high-resolution 3D seismic data acquired offshore Montserrat, Lesser Antilles. Marine Geology, 335, 1-15, https://doi.org/10.1016/j.margeo.2012.10.004

Druitt, T. H., Edwards, L., Mellors, R. M., Pyle, D. M., Sparks, R. S. J., Lanphere, M., ... & Barreirio, B. (1999). Santorini volcano. Geological Society Memoir, 19

Druitt, T. H., McCoy, F. W., & Vougioukalakis, G. E. (2019). The late bronze age eruption of Santorini volcano and its impact on the ancient Mediterranean world. Elements: An International Magazine of Mineralogy, Geochemistry, and Petrology, 15(3), 185-190, https://doi.org/10.2138/gselements.15.3.185

Feuillet, N., 2013. The 2011–2012 unrest at Santorini rift: stress interaction between active faulting and volcanism. Geophys. Res. Lett. 40 (14), 3532–3537, https://doi.org/10.1002/grl.50516

Frey-Martinez, J., Cartwright, J., & James, D. (2006). Frontally confined versus frontally emergent submarine landslides: A 3D seismic characterisation. Marine and Petroleum Geology, 23(5), 585-604, https://doi.org/10.1016/j.marpetgeo.2006.04.002

Harjono, H., Diament, M., Dubois, J., Larue, M., & Zen, M. T. (1991). Seismicity of the Sunda Strait: evidence for crustal extension and volcanological implications. Tectonics, 10(1), 17-30, https://doi.org/10.1029/90TC00285

Heath, B. A., Hooft, E. E. E., Toomey, D. R., Papazachos, C. B., Nomikou, P., Paulatto, M., ... & Warner, M. R. (2019). Tectonism and its relation to magmatism around Santorini Volcano from upper crustal P wave velocity. Journal of Geophysical Research: Solid Earth, 124(10), 10610-10629, https://doi.org/10.1029/2019JB017699

Hooft, E. E., Nomikou, P., Toomey, D. R., Lampridou, D., Getz, C., Christopoulou, M. E., ... & Van der Beek, B. P. (2017). Backarc tectonism, volcanism, and mass wasting shape seafloor morphology in the Santorini-Christiana-Amorgos region of the Hellenic Volcanic Arc. Tectonophysics, 712, 396-414.hemistry, and Petrology, 15(3), 185-190, https://doi.org/10.1016/j.tecto.2017.06.005

Hooft, E. E. E., Heath, B. A., Toomey, D. R., Paulatto, M., Papazachos, C. B., Nomikou, P., ... & Warner, M. R. (2019). Seismic imaging of Santorini: Subsurface constraints on caldera

collapse and present-day magma recharge. Earth and Planetary Science   Letters, 514, 48-61, https://doi.org/10.1016/j.epsl.2019.02.033

Hübscher, C., Hensch, M., Dahm, T., Dehghani, A., Dimitriadis, I., Hort, M., & Taymaz, T.   (2006). Toward a risk assessment of central Aegean volcanoes. Eos, Transactions American Geophysical Union, 87(39), 401-407,   https://doi.org/10.1029/2006EO390002

Hübscher, C., Ruhnau, M., & Nomikou, P. (2015). Volcano-tectonic evolution of the
        polygenetic Kolumbo submarine volcano/Santorini (Aegean Sea). Journal of
        Volcanology and Geothermal Research, 291, 101-111,
        https://doi.org/10.1016/j.jvolgeores.2014.12.020

Hunt, J. E., Cassidy, M., & Talling, P. J. (2018). Multi-stage volcanic island flank collapses with
        coeval explosive caldera-forming eruptions. Scientific reports, 8(1), 1-11,
        https://doi.org/10.1038/s41598-018-19285-2

Hutchison, A. A., Cashman, K. V., Williams, C. A., & Rust, A. C. (2016). The 1717 eruption of
        Volcán de Fuego, Guatemala: cascading hazards and societal response. Quaternary
        International, 394, 69-78, https://doi.org/10.1016/j.quaint.2014.09.050

Ida, Y., & Voight, B. (1995). Models of magmatic processes and volcanic eruptions. Journal of
        volcanology and geothermal research, 66(1-4),
        https://doi.org/10.1016/0377-0273(95)00000-K

Kamata, H., & Kodama, K. (1999). Volcanic history and tectonics of the Southwest Japan Arc.
        Island Arc, 8(3), 393-403, https://doi.org/10.1046/j.1440-1738.1999.00241.x

Karstens, J., Crutchley, G. J., Berndt, C., Talling, P. J., Watt, S. F., Hühnerbach, V., ... &
        Trofimovs, J. (2013). Emplacement of pyroclastic deposits offshore Montserrat: Insights from 3D seismic data. Journal of volcanology and geothermal research, 257,   1-11, https://doi.org/10.1016/j.jvolgeores.2013.03.004

Karstens, J., Crutchley, G., Elger, J., Kühn, M., Schmid, F., Dalla Valle, G., ... & Nomikou, P.
        (2020). R/V Poseidon Cruise Report 538-THESEUS Tsunami hazard of explosive
        submarine eruptions, 15th July–26th July, 2019 Cartagena (Spain)-Heraklion
        (Greece), http://oceanrep.geomar.de/id/eprint/49501

Karstens, J., Berndt, C., Urlaub, M., Watt, S. F., Micallef, A., Ray, M., ... & Brune, S. (2019).
        From gradual spreading to catastrophic collapse–Reconstruction of the 1888 Ritter

Island volcanic sector collapse from high-resolution 3D seismic data. Earth and Planetary Science Letters, 517, 1-13, https://doi.org/10.1016/j.epsl.2019.04.009

Kühn, M., Karstens, J., Berndt, C., & Watt, S. F. (2021). Seismic reconstruction of seafloor sediment deformation during volcanic debris avalanche emplacement offshore Sakar, Papua New Guinea. Marine Geology, https://doi.org/10.1016/j.margeo.2021.106563

Kutterolf, S., Freundt, A., Druitt, T. H., McPhie, J., Nomikou, P., Pank, K., ... & Allen, S. R. (2021a). The medial offshore record of explosive volcanism along the central to eastern Aegean Volcanic Arc: 2. Tephra ages and volumes, eruption magnitudes and marine sedimentation rate variations. Geochemistry, Geophysics, Geosystems, 22(12), https://doi.org/10.1029/2021GC010010.

Kutterolf, S., Freundt, A., Druitt, T. H., McPhie, J., Nomikou, P., Pank, K., ... & Allen, S. R. (2021b). The medial offshore record of explosive volcanism along the central to eastern Aegean Volcanic Arc: 2. Tephra ages and volumes, eruption magnitudes and marine sedimentation rate variations. Geochemistry, Geophysics, Geosystems, 22(12), https://doi.org/10.1029/2021GC010011.

Le Friant, A., Harford, C. L., Deplus, C., Boudon, G., Sparks, R. S. J., Herd, R. A., & Komorowski, J. C. (2004). Geomorphological evolution of Montserrat (West Indies): importance of flank collapse and erosional processes. Journal of the Geological Society, 161(1), 147- 160, https://doi.org/10.1144/0016-764903-017

Le Friant, A., Ishizuka, O., Boudon, G., Palmer, M. R., Talling, P. J., Villemant, B., ... & Watt, S. F. L. (2015). Submarine record of volcanic island construction and collapse in the Lesser A ntilles arc: First scientific drilling of submarine volcanic island landslides by IODP E xpedition 340. Geochemistry, Geophysics, Geosystems, 16(2), 420-442, https://doi.org/10.1002/2014GC005652

Le Friant, A., Lebas, E., Brunet, M., Lafuerza, S., Hornbach, M., Coussens, M., ... & IODP 340 Expedition Science Party. (2019). Submarine landslides around volcanic islands: A review of what can be learned from the Lesser Antilles Arc. Submarine Landslides: Subaqueous Mass Transport Deposits from Outcrops to Seismic Profiles, 277-297, https://doi.org/10.1002/9781119500513.ch17

Le Pichon, X., & Angelier, J. (1981). The Aegean Sea. Philosophical Transactions of the Royal Society of London. Series A, Mathematical and Physical Sciences, 300(1454), 357-372, https://doi.org/10.1098/rsta.1981.0069

Lebas, E., Le Friant, A., Boudon, G., Watt, S. F. L., Talling, P. J., Feuillet, N., ... & Vardy, M. E. (2011). Multiple widespread landslides during the long-term evolution of a volcanic island: Insights from high-resolution seismic data, Montserrat, Lesser Antilles. Geochemistry, Geophysics, Geosystems, 12(5), https://doi.org/10.1029/2010GC003451

López-Saavedra, M., Martí, J., Rubio, J. L., & Kelfoun, K. (2021). Cascading Effects of Extreme Geohazards on Tenerife (Canary Islands). Journal of Geophysical Research: Solid Earth, 126(9), e2021JB022294, https://doi.org/10.1029/2021JB022294

Løvholt, F., Pedersen, G., & Gisler, G. (2008). Oceanic propagation of a potential tsunami from the La Palma Island. Journal of Geophysical Research: Oceans, 113 (C9), https://doi.org/10.1029/2007JC004603

Manconi, A., Longpré, M. A., Walter, T. R., Troll, V. R., & Hansteen, T. H. (2009). The effects of flank collapses on volcano plumbing systems. Geology, 37(12), 1099-1102, https://doi.org/10.1130/G30104A.1

Masson, D. G., Watts, A. B., Gee, M. J. R., Urgeles, R., Mitchell, N. C., Le Bas, T. P., & Canals, M. (2002). Slope failures on the flanks of the western Canary Islands. Earth-Science Reviews, 7(1-2), 1- 35, https://doi.org/10.1016/S0012-8252(01)00069-1

McGuire, W. J. (1996). Volcano instability: a review of contemporary themes. Geological Society, London, Special Publications, 110(1), 1-23,   https://doi.org/10.1144/GSL.SP.1996.110.01.01

Mitchum Jr, R. M., Vail, P. R., & Thompson III, S. (1977). Seismic stratigraphy and global   changes of sea level: Part 2. The depositional sequence as a basic unit for   stratigraphic analysis: Section 2. Application of seismic reflection configuration to stratigraphic interpretation, https://doi.org/10.1306/M26490C9

Moore, J. G., Normark, W. R., & Holcomb, R. T. (1994). Giant hawaiian landslides. Annual Review of Earth and Planetary Sciences, 22, 119-144.

Moore, J. G., Clague, D. A., Holcomb, R. T., Lipman, P. W., Normark, W. R., & Torresan, M. E. (1989). Prodigious submarine landslides on the Hawaiian ridge. Journal of

Geophysical Research, 94(B12), 17,465–17, 48,

https://doi.org/10.1029/JB094iB12p17465

Nomikou, P., Carey, S., Papanikolaou, D., Bell, K. C., Sakellariou, D., Alexandri, M., & Bejelou,

K. (2012). Submarine volcanoes of the Kolumbo volcanic zone NE of Santorini   Caldera,

Greece. Global and Planetary Change, 90, 135-151.,

https://doi.org/10.1016/j.gloplacha.2012.01.001

Nomikou, P., Papanikolaou, D., Alexandri, M., Sakellariou, D., & Rousakis, G. (2013).

Submarine volcanoes along the Aegean volcanic arc. Tectonophysics, 597, 123-146,

https://doi.org/10.1016/j.tecto.2012.10.001

Nomikou, P., Druitt, T. H., Hübscher, C., Mather, T. A., Paulatto, M., Kalnins, L. M., ... & Parks,

M. M. (2016a). Post-eruptive flooding of Santorini caldera and implications for   tsunami

generation. Nature   communications, 7(1), 1-10,   https://doi.org/10.1038/ncomms13332

(2016)

Nomikou, P., Hübscher, C., Ruhnau, M., & Bejelou, K. (2016b). Tectono-stratigraphic

evolution through successive extensional events of the Anydros Basin, hosting   Kolumbo

volcanic field at the Aegean Sea, Greece. Tectonophysics, 671, 202-217,

https://doi.org/10.1016/j.tecto.2016.01.021

Nomikou, P., Hübscher, C., Papanikolaou, D., Farangitakis, G. P., Ruhnau, M., & Lampridou,

D. (2018). Expanding extension, subsidence and lateral segmentation within the

Santorini-Amorgos basins during Quaternary: Implications for the 1956 Amorgos events,

central-south Aegean Sea, Greece. Tectonophysics, 722, 138-153,

https://doi.org/10.1016/j.tecto.2017.10.016

Nomikou, P., Hübscher, C., & Carey, S. (2019). The Christiana–Santorini–Kolumbo Volcanic

Field. Elements: An International Magazine of Mineralogy, Geochemistry, and

Petrology, 15(3), 171-176, https://doi.org/10.2138/gselements.15.3.171

Ogata, K., Mountjoy, J. J., Pini, G. A., Festa, A., & Tinterri, R. (2014). Shear zone liquefaction

in mass transport deposit emplacement: a multi-scale integration of seismic

reflection and outcrop data. Marine Geology, 356, 50-64,

https://doi.org/10.1016/j.margeo.2014.05.001

Pareschi, M. T., Boschi, E., Mazzarini, F., & Favalli, M. (2006). Large submarine landslides offshore Mt. Etna. Geophysical Research Letters, 33(13), https://doi.org/10.1029/2006GL026064

Patrick, M. R., Houghton, B. F., Anderson, K. R., Poland, M. P., Montgomery-Brown, E., Johanson, I., ... & Elias, T. (2020). The cascading origin of the 2018 Kīlauea eruption and implications for future forecasting. Nature Communications, 11(1), 1-13,

Pinel, V., & Albino, F. (2013). Consequences of volcano sector collapse on magmatic storage zones: Insights from numerical modeling. Journal of volcanology and geothermal research, 252, 29- 37, https://doi.org/10.1016/j.jvolgeores.2012.11.009

Piper, D. J. W., & Perissoratis, C. (2003). Quaternary neotectonics of the South Aegean arc. Marine Geology, 198(3-4), 259-288, https://doi.org/10.1016/S0025-3227(03)00118-X

Posamentier, H. W., Martinsen, O. J., & Shipp, R. C. (2011). The character and genesis of submarine mass-transport deposits: insights from outcrop and 3D seismic data. Mass-transport deposits in deepwater settings. Tulsa: SEPM, Special Publication, 96, 7-38, https://doi.org/10.2110/sepmsp.096.007.

Preine, J., Karstens, J., Hübscher, C., Nomikou, P., Schmid, F., Crutchley, G., Papanikolaou, D., Druitt, T. (2022). Spatio-Temporal Evolution of the Christiana-Santorini-Kolumbo Volcanic Field, Aegean Sea. Geology, https://doi.org/10.1130/G49167.1

Preine, J., Schwarz, B., Bauer, A., & Hübscher, C. (2020). When There Is No Offset: A Demonstration of Seismic Diffraction Imaging and Depth-Velocity Model Building in the Southern Aegean Sea. Journal of Geophysical Research: Solid Earth, 125(9), https://doi.org/10.1029/2020JB019961

Priyanto, W. S., Hunt, J. E., Hanif, M., Tappin, D. R., Permana, H., Cassidy, M., & Yulianto, E. (2021). Bathymetry and shallow seismic imaging of the 2018 flank collapse of Anak Krakatau. Frontiers in Earth Science, 649, https://doi.org/10.3389/feart.2020.577448

Satow, C., Gudmundsson, A., Gertisser, R., Ramsey, C. B., Bazargan, M., Pyle, D. M., ... & Hardiman, M. (2021). Eruptive activity of the Santorini Volcano controlled by sea-level rise and fall. Nature Geoscience, 14(8), 586-592, https://doi.org/10.1038/s41561-021-00783-4

Sawyer, D. E., P. B. Flemings, B. Dugan, and J. T. Germaine (2009), Retrogressive failures recorded in mass transport deposits in the Ursa Basin, Northern Gulf of Mexico, J. Geophys. Res., 114, B10102, https://doi.org/10.1029/2008JB006159.

Siebert, L. (1984). Large volcanic debris avalanches: characteristics of source areas, deposits, and associated eruptions. Journal of volcanology and geothermal research, 22(3-4), 163-197, https://doi.org/10.1016/0377-0273(84)90002-7

Sigurdsson, H., Carey, S., Alexandri, M., Vougioukalakis, G., Croff, K., Roman, C., ... & Nomikou, P. (2006). Marine investigations of Greece's Santorini volcanic field. EOS, Transactions American Geophysical Union, 87(34), 337-342, https://doi.org/10.1029/2006EO340001

Smit, F. W., & Stemmerik, L. (2022). Seismic geomorphology of submarine landslides in the Chalk Group of the Danish Central Graben–implications for reservoir potential. Geological Society, London, Special Publications, 525, https://doi.org//10.1144/SP525-2020-244

Sørensen, M. B., Spada, M., Babeyko, A., Wiemer, S., & Grünthal, G. (2012). Probabilistic tsunami hazard in the Mediterranean Sea. Journal of Geophysical Research: Solid Earth, 117(B1), https://doi.org/10.1029/2010JB008169

Tatsumi, Y., Suzuki-Kamata, K., Matsuno, T., Ichihara, H., Seama, N., Kiyosugi, K., ... & Yamamoto, Y. (2018). Giant rhyolite lava dome formation after 7.3 ka supereruption at Kikai caldera, SW Japan. Scientific Reports, 8(1), 1-9, https://doi.org/10.1038/s41598-018-21066-w

Tsampouraki-Kraounaki, K., & Sakellariou, D. (2018). Seismic stratigraphy and geodynamic evolution of Christiana Basin, South Aegean arc. Marine Geology, 399, 135-147, https://doi.org/10.1016/j.margeo.2018.02.012

Urgeles, R., & Camerlenghi, A. (2013). Submarine landslides of the Mediterranean Sea: Trigger mechanisms, dynamics, and frequency-magnitude distribution. Journal of Geophysical Research: Earth Surface, 118(4), 2600-2618, https://doi.org/10.1002/2013JF002720

Viesca, R. C., & Rice, J. R. (2012). Nucleation of slip-weakening rupture instability in landslides by localized increase of pore pressure. Journal of Geophysical Research: Solid Earth, 117(B3), https://doi.org/10.1029/2011JB008866

Voight, B. (2000). Structural stability of andesite volcanoes and lava domes. Philosophical
Transactions of the Royal Society of London. Series A: Mathematical, Physical and
Engineering Sciences, 358(1770), 1663-1703, https://doi.org/10.1098/rsta.2000.0609

Walter, T. R., Haghighi, M. H., Schneider, F. M., Coppola, D., Motagh, M., Saul, J., ... & Gaebler,
P. (2019). Complex hazard cascade culminating in the Anak Krakatau sector collapse.
Nature communications, 10(1), 1-11,
https://doi.org/10.1038/s41467-019-12284-5

Watt, S. F. L., Talling, P. J., Vardy, M. E., Heller, V., Hühnerbach, V., Urlaub, M., ... & Maeno,
F. (2012). Combinations of volcanic-flank and seafloor-sediment failure offshore Montserrat,
and their implications for tsunami generation. Earth and Planetary Science Letters, 319,
228-240, https://doi.org/10.1016/j.epsl.2011.11.032

Watt, S. F. L., Karstens, J., Micallef, A., Berndt, C., Urlaub, M., Ray, M., ... & Elger, J. (2019).
From catastrophic collapse to multi-phase deposition: flow transformation, seafloor
interaction and triggered eruption following a volcanic-island landslide. Earth and
Planetary Science Letters, 517, 135-147, https://doi.org/10.1016/j.epsl.2019.04.024

Watt S. F. L., Karstens J, Berndt C (2021) Volcanic-Island Lateral Collapses and Their
Submarine Deposits. In: Roverato M, Dufresne A, Procter J (eds) Volcanic Debris
Avalanches: From Collapse to Hazard. Advances in Volcanology Book Series. Springer
International Publishing, Cham, pp 255-279 https://doi.org/10.1007/978-3-030-
57411-6_10

Zuccaro, G., De Gregorio, D., & Leone, M. F. (2018). Theoretical model for cascading effects
analyses. International journal of disaster risk reduction, 30, 199-215,
https://doi.org/10.1016/j.ijdrr.2018.04.019

Figure Captions:

Figure 1: A) Regional setting of the Southern Aegean Sea, showing the Hellenic Volcanic Arc and the study area (blue box). B) Morphological map of the CSKVF showing islands, basins, volcanic centers, and major extensional structures (red lines) after Nomikou et al. (2016b, 2018, 2019). Coordinate system is UTM Zone 35N, WGS84. Grey lines show all seismic profiles, white lines indicate the locations of seismic profiles shown in this study. Dashed white rectangle indicates the location of the 3D view of Christiana shown in Fig. 3G. Bathymetry from Nomikou et al. (2012, 2013, 2018, 2019) and Hooft et al. (2017). Topography from the Hellenic Military Geographic Service (HMGS).

Figure 2: Summary of the seismic facies of Units 3-6 with four subunits identified within U4. Horizons h4, h5, and h6 (green, orange, and blue lines) are the basal reflectors of the corresponding units (U4-U6) as established in Preine et al. (2022). Seismic facies based on concepts of Mitchum et al. (1977) and interpretation based on Bull et al. (2009) and Smit et al. (2022).

Figure 3: A) Seismic line connecting single-channel and high-resolution multichannel seismic lines across the Christiana Basin and the western flank of Santorini. Labels U3-U6 represent Units 3-6 and U4a-d represent subunits of Unit 4 as outlined in Figure 2. Horizons h4, h5, and h6 (green, orange, and blue lines) are the basal reflectors of the corresponding units (U4-U6). TPF = Thera Pyroclastic Formation. Poseidon indicates volcanoclastic deposits from the eponymous volcanic center according to Preine et al. (2022). B) High-resolution multichannel seismic profile crossing the Christiana Basin and the incised northeastern flank of the Christiana Edifice. A weak and disrupted base of U4 is marked by the broken red line, as opposed to the green line (h4), which represents a distinct and continuous basal reflection. C) High-resolution multichannel seismic profile crossing the Christiana Basin, the Christiana Fault, and volcanic domes adjacent to Chrisitana. Black lines are normal faults. D) Map showing the thickness of Unit 4 and the location of the profiles. Toothed black line is the Christiana Fault. E), F) Enlargements from the seismic profile shown in B. G) 3D view of the Christiana Edifice and the Christiana Fault scar (5 times vertically exaggerated).

Figure 4: A) High-resolution seismic profile crossing the western Santorini-Anafi Basin. Horizon and unit labels as in Figure 3. TPF = Thera Pyroclastic Formation. B) High-resolution seismic profile crossing the southeastern slope of Santorini. C) Map showing the thickness of the chaotic deposit (Unit 4) and the location of the profiles. D, E) Enlargements from the seismic profile shown in B.

Figure 5: A) High-resolution seismic profile crossing the Anhydros Basin in NW-SE direction towards the Kolumbo Edifice. K1-K5 represent different episodes of cone growth following Hübscher et al. (2015) and Preine et al. (2022). Horizon and unit labels as in Figure 3. TPF = Thera Pyroclastic Formation. B) High-resolution seismic profile crossing the Anhydros Basin in SW-NE direction. C) Map showing the thickness of Unit 4 and the locations of the profiles.

Figure 6: A) Seismic profile crossing the Anhydros and Santorini-Anafi Basins. Horizon and Unit labels as in Figure 3. B, C) Enlargements highlight the internal architecture of Unit 4, which is onlapping the main faults towards the northwest and reflection h4 towards the southeast. D) TWT thickness map of Unit 4 with the location of the seismic profile.
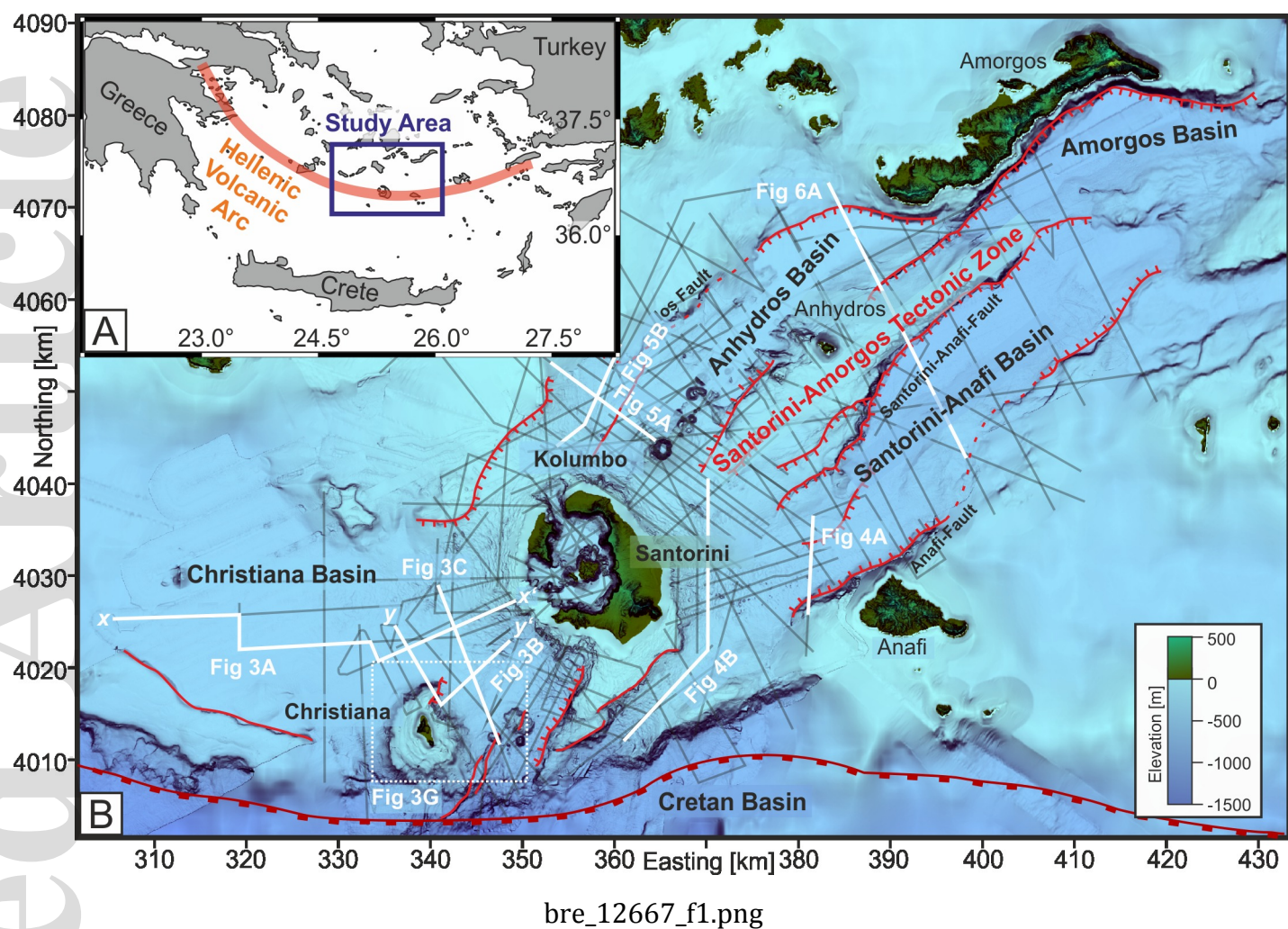
Figure 7: Enlargements of Unit 4 from each basin illustrating the stratigraphic correlation. The enlargement from the eastern Santorini-Anafi Basin is flipped compared to Fig. 6. Horizon and unit labels as in Figures 3-6. For locations, see the boxes in Figures 3-6.

Figure 8: A) TWT depth map of the base of Unit 4. B) TWT thickness map of Unit 4. Both maps are based on the interpolated seismic profiles shown in light grey. Red lines indicate faults from Nomikou et al. (2016b; 2018; 2019); black lines indicate faults from this study. Dashed lines in B indicate individual depo-centers, labeled I-VIII.
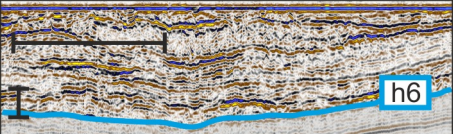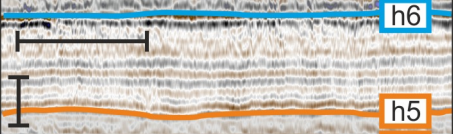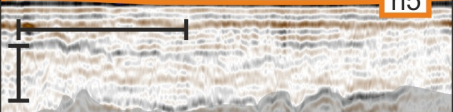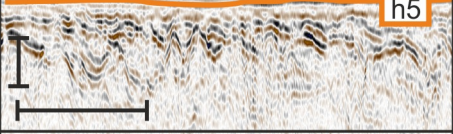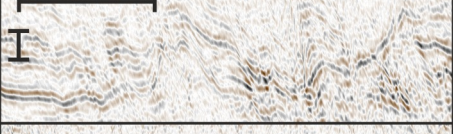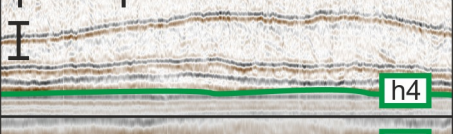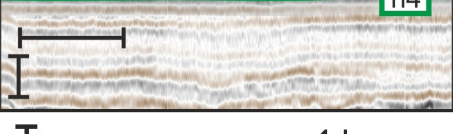
Figure 9: Enlarged view of internal reflections within Unit 4 (between horizons h5 and h4) in the Christiana (A) and western Santorini-Anafi Basin (B). PR: Phase Reversal. Subunits (U4a, U4c) as introduced in Figure 2.

Figure 10: Enlarged view of Unit 4 (colored semi-transparent orange) in front of the Ios Fault in the Anhydros Basin (A), in front of the Anhydros Fault in the Eastern Santorini-Anafi Basin (B), and in front of the Santorini-Anafi Fault in the Western Santorini-Anafi Basin (C). Horizon and Unit labels as in Figure 3. (D) Thickness map as in Figure 8B with locations of profiles 10A-C. IF: Ios Fault; AF: Anhydros Fault; SAF: Santorini-Anafi Fault.

Figure 11: Schematic Reconstruction of the Santorini Mass Transport Cascade (SMTC) forming the Santorini Mass-Transport Deposit (SMTD). Topographic highs are indicated by the grey areas. Present-day coastlines for approximate reference. Light red color schematically highlights areas with increased tectonic activity or instability. Approximate ages from Preine et al. (2022). (A) Location of volcanic centers prior to the emplacement of the SMTD. (B) Rift pulse affecting the entire Christiana-Santorini-Kolumbo Field. CF: Christiana Fault; SSF: Southern Santorini Fault; SAF: Santorini-Anafi Fault; KF: Kolumbo Fault; IF: Ios Fault; AF: Anhydros Fault. (C) Precursory Mass-Transport Events (green) occur due to tectonic activity. (D) Catastrophic sector collapses (red) occur at Christiana and the south-eastern flank of Santorini. (E) Due to the sudden seafloor loading caused by the sector collapses, a décollement propagates along the flank of Santorini triggering large-scale secondary sediment failures (blue). (F) Emerging volcanic centers (orange, Preine et al., 2022) after the emplacement of the SMTD.
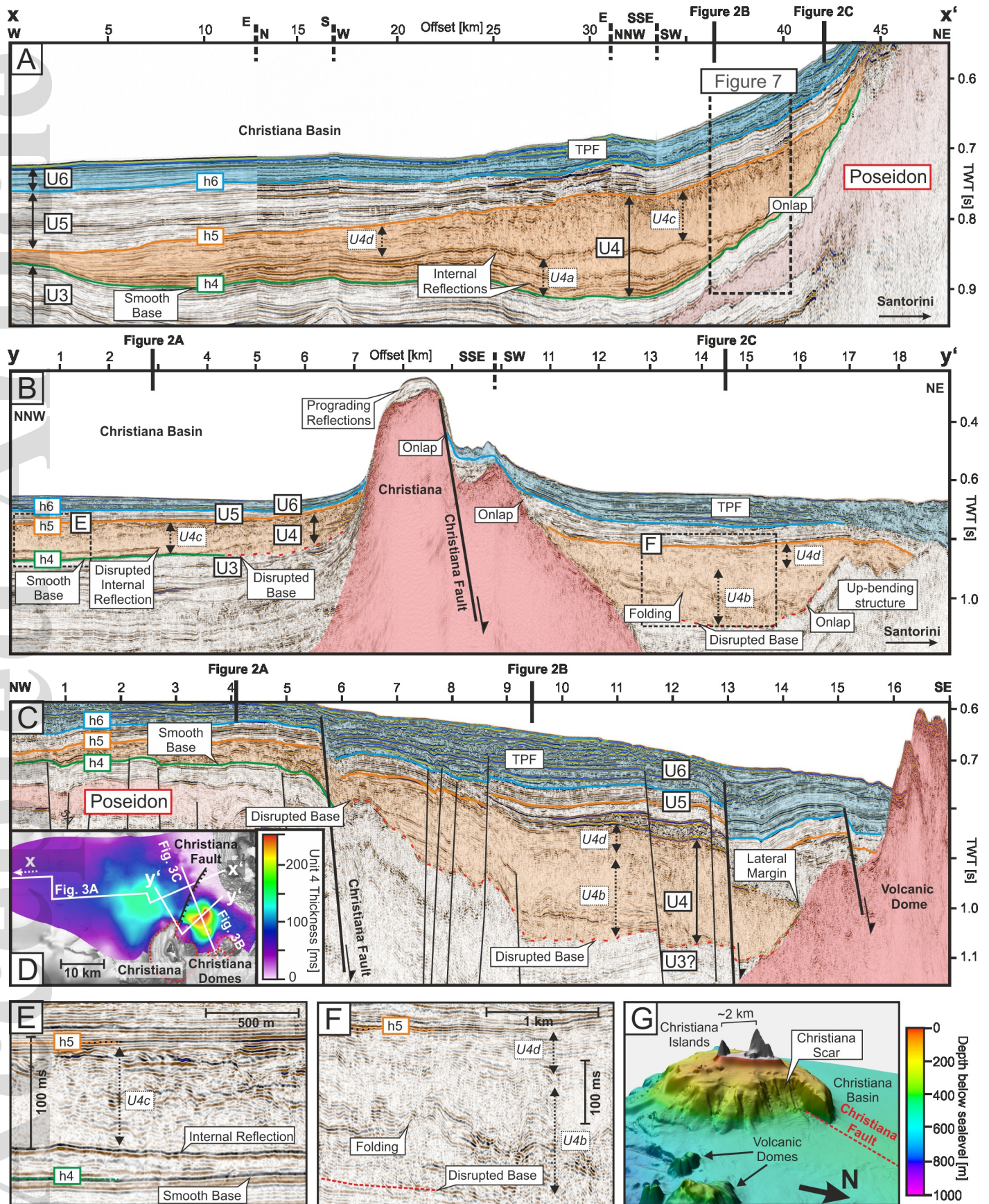
bre_12667_f1.png

| Unit	Sub-Unit	Illustration	Reflection configuration	Interpretation	Figures	
U6	-		Subparallel reflections of moderate amplitudes intercalated with hummocky, chaotic, high-amplitude reflections	Volcanic deposits from Santorini	3A,B,C 4A,B,D,E 5A,B 6A,B	7 9 10
U5	-		Parallel, low-amplitude reflections	Hemipelagic sedimentation	3A-C,E,F 4A,B,D,E 5A,B 6A,B,C	7 9 10
U4	U4d		Subparallel coherent to incoherent reflections with low amplitudes	Turbidity flow deposits	3A,B,C,F 5A,B 6A,B,C 7	
	U4c		Incoherent, transparent facies with some scattered reflection patches and wavy reflections at the top	Debris flow deposits	3A-CF 5A,B 6A,C 7	7 9 10
	U4b		Chaotic and deformed reflections with moderate amplitudes interrupted by some partially layered reflection sequences	Slump deposits	3B,C,F 4B,D,E	
	U4a		Subparallel to irregular, high-amplitude internal reflections	Stacked mass-transport deposits	3A,B,E 4A 5A,B 6A,B,C	7 9 10
U3	-		Parallel, low-amplitude reflections	Hemipelagic sedimentation	3A,B,C,E 4A,B,D,E 5A,B 6A,B,C	7 9 10

25 ms TWT   1 km

bre_12667_f2.png

bre_12667_f3.png
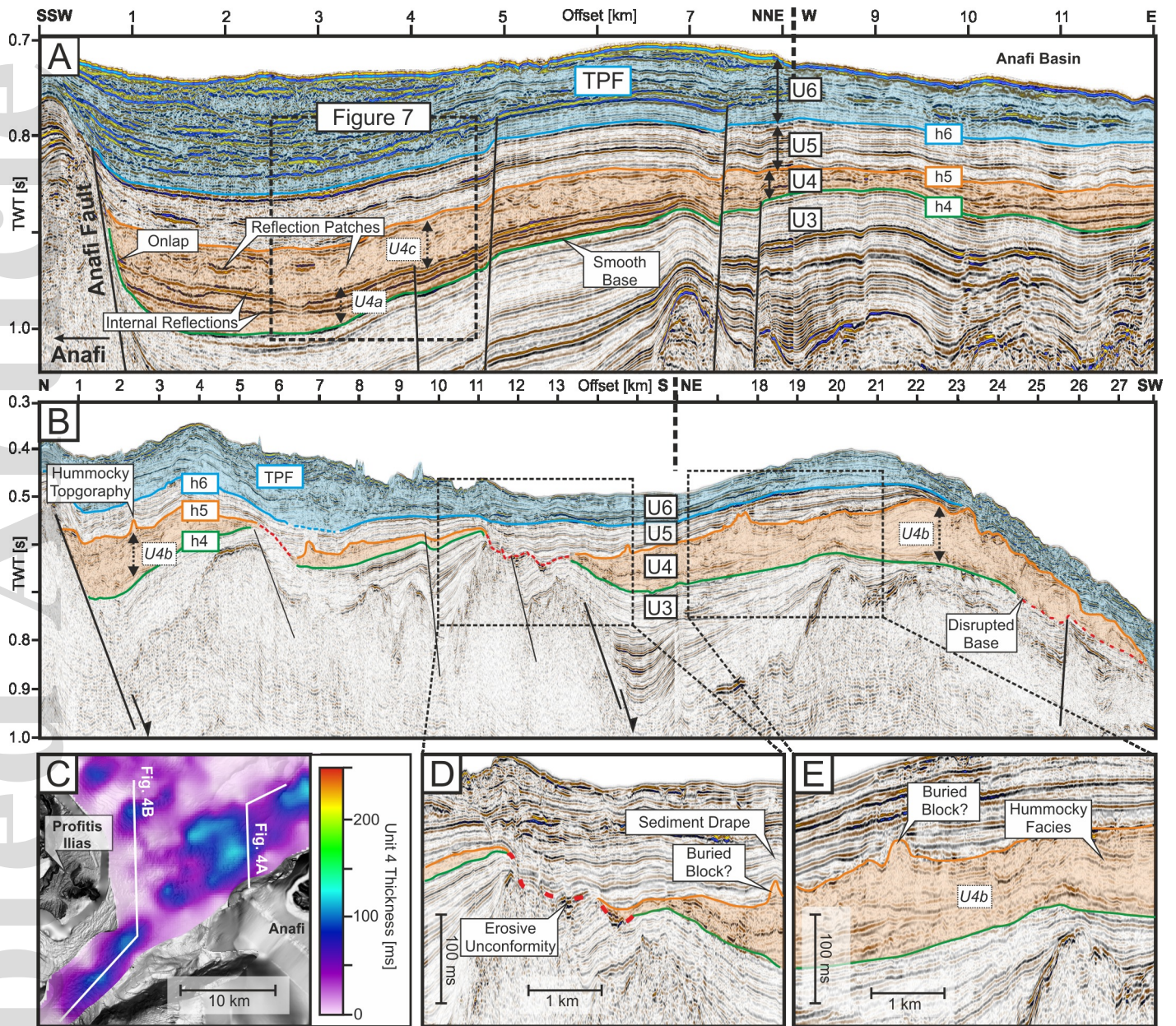
bre_12667_f4.png
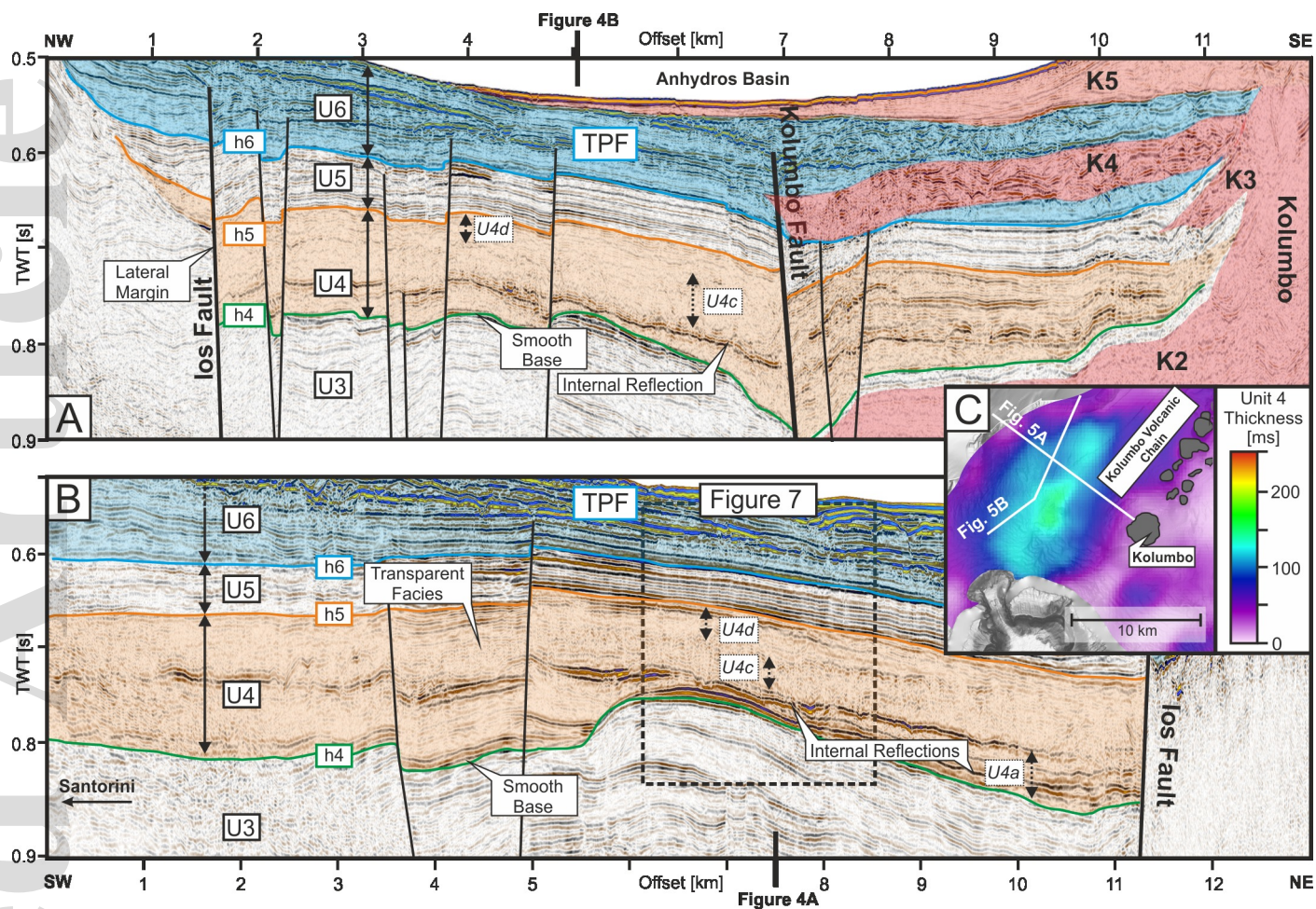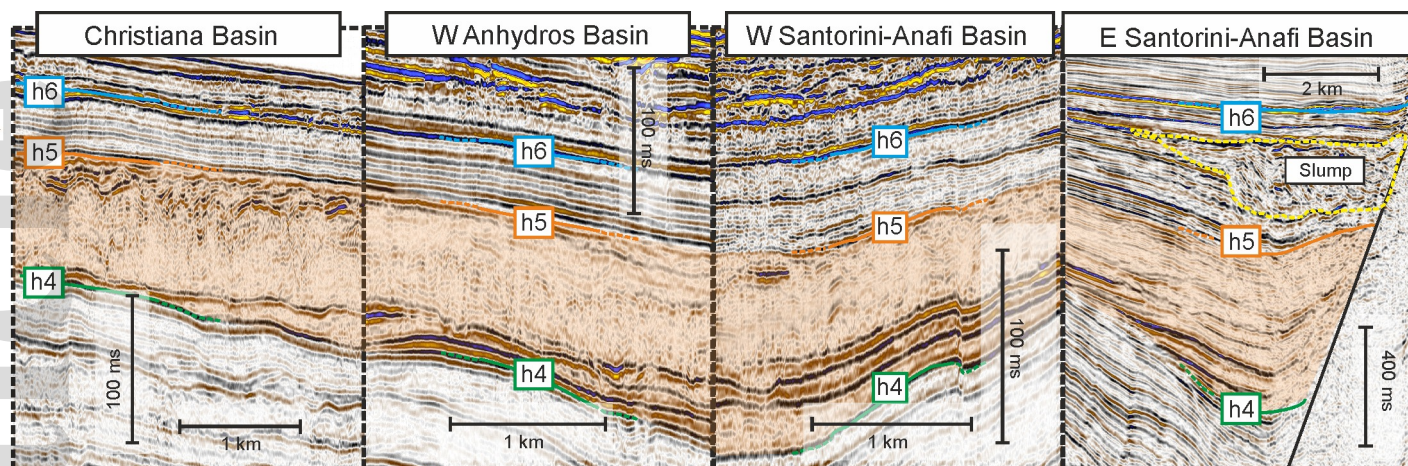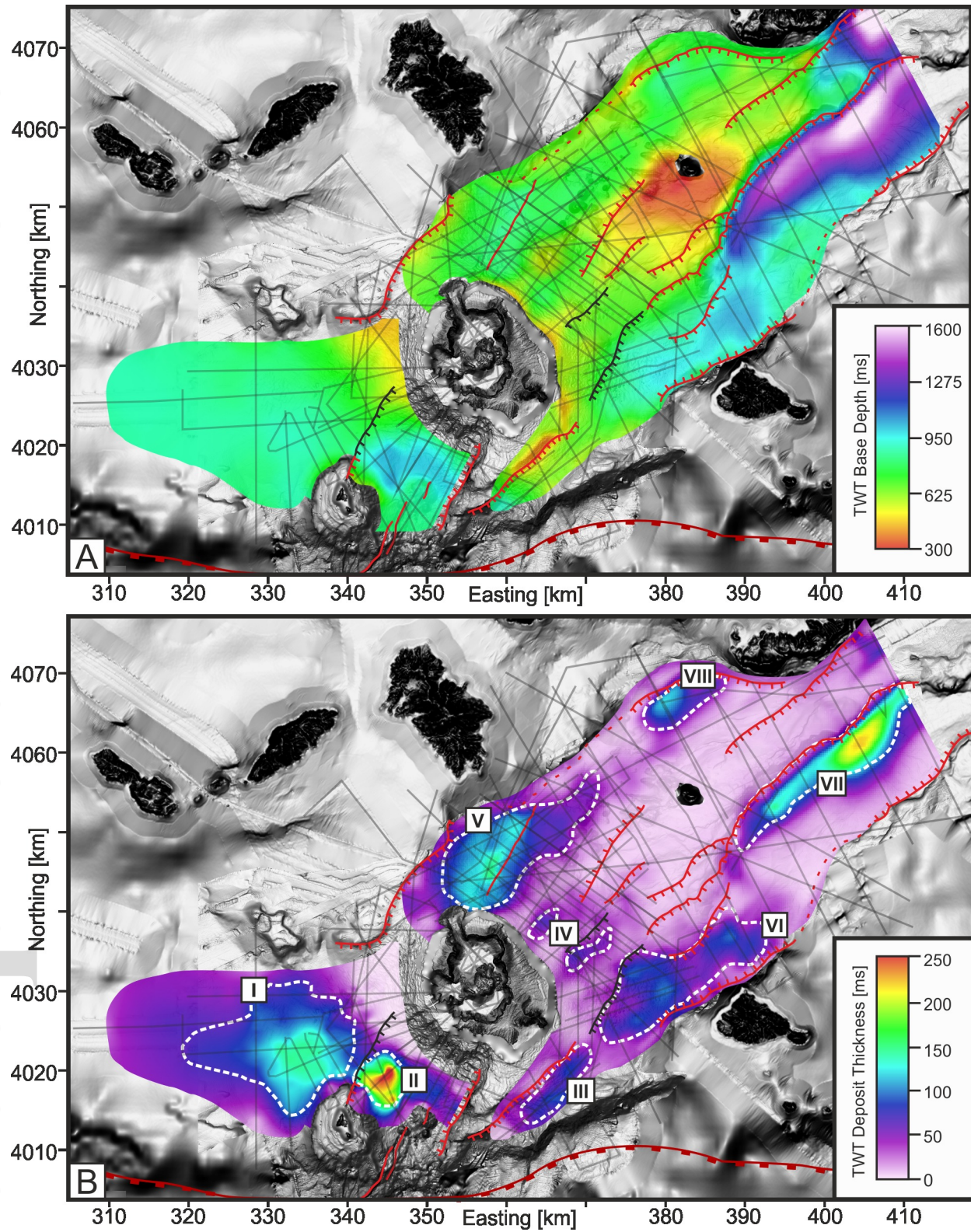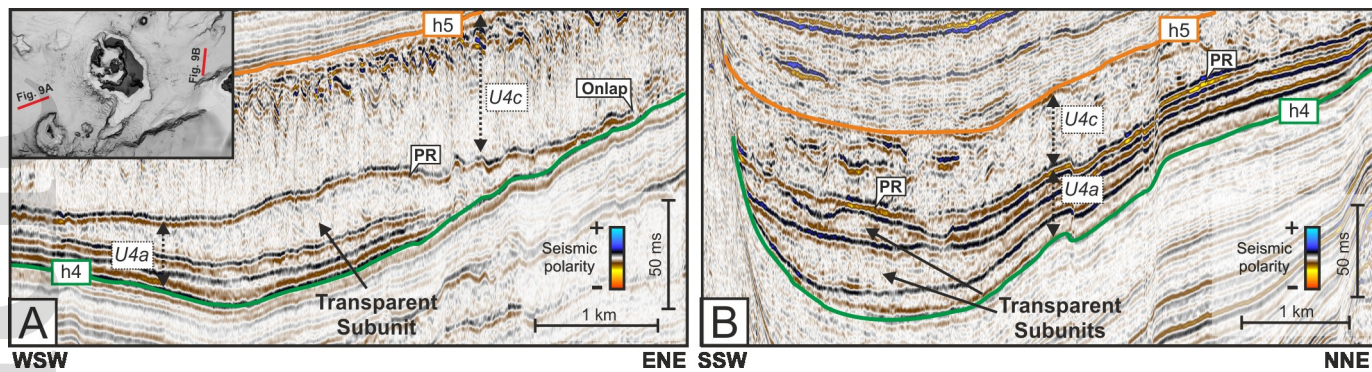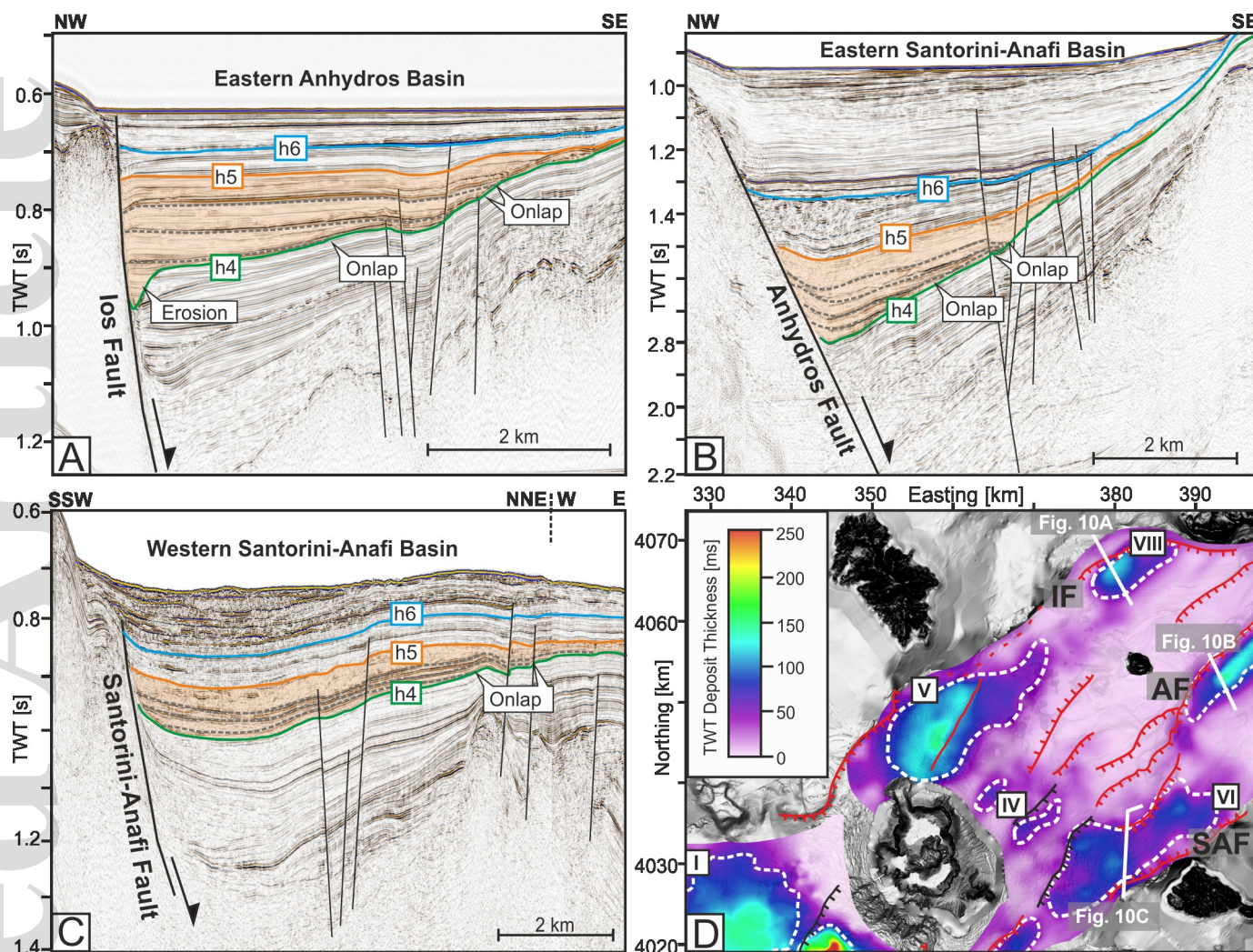
bre_12667_f5.png
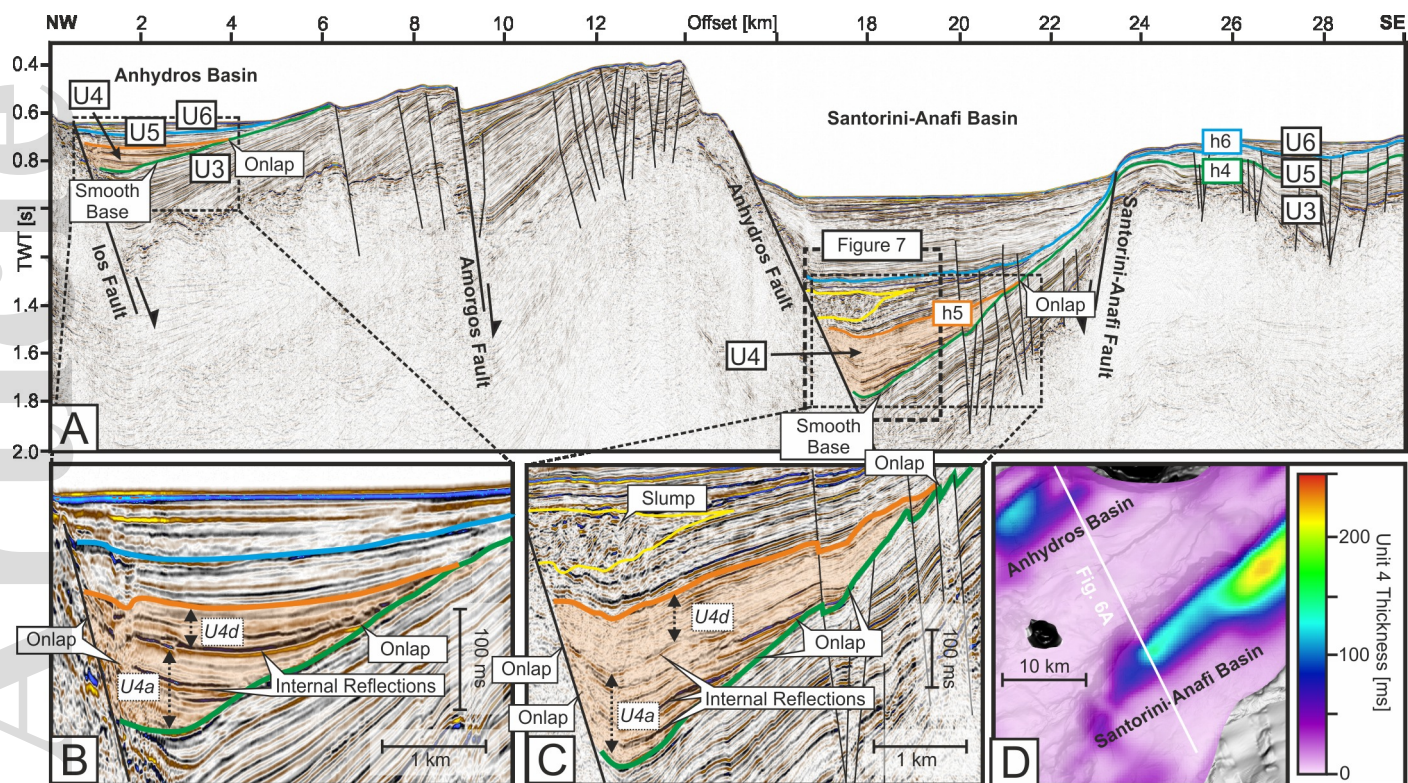
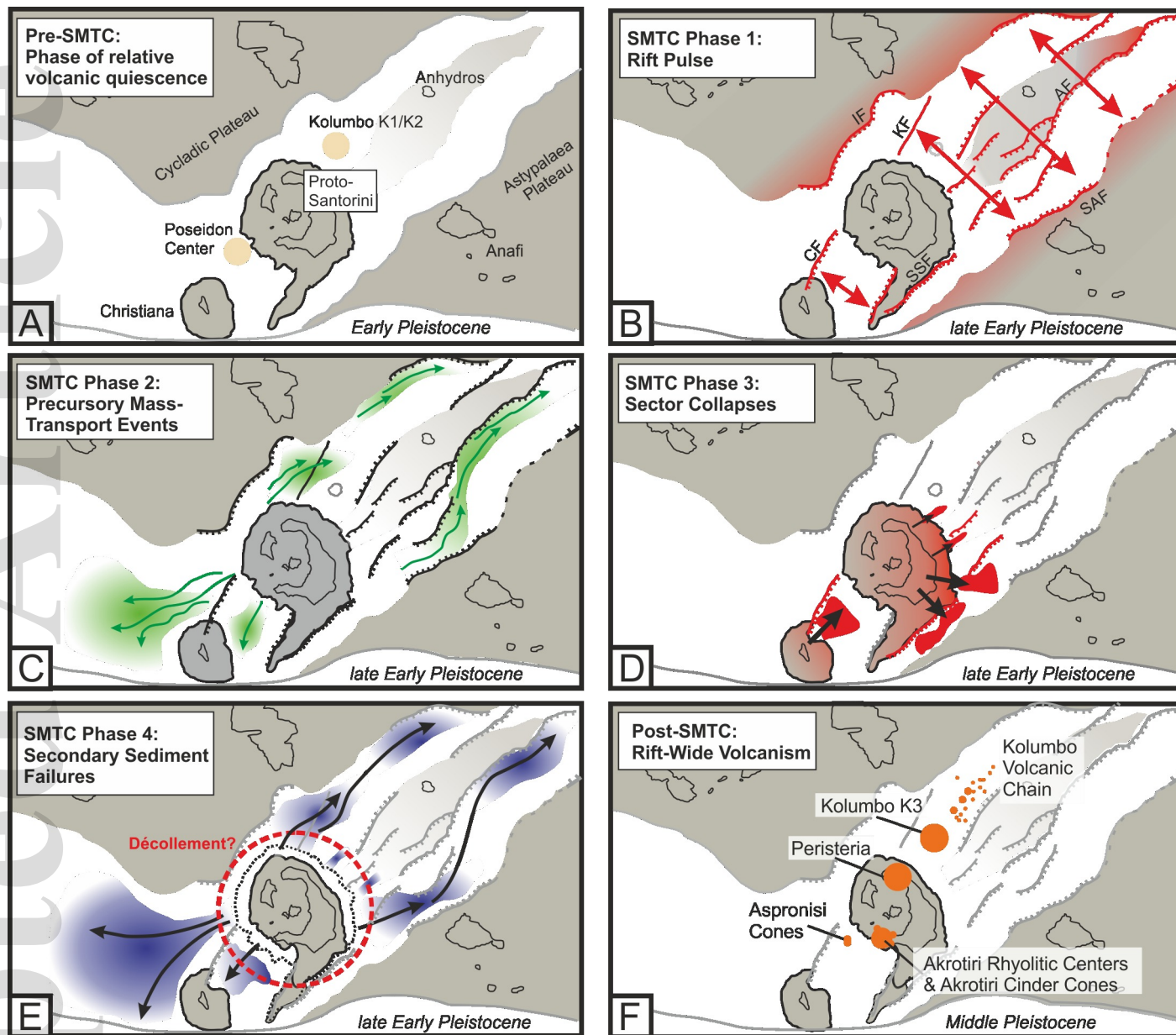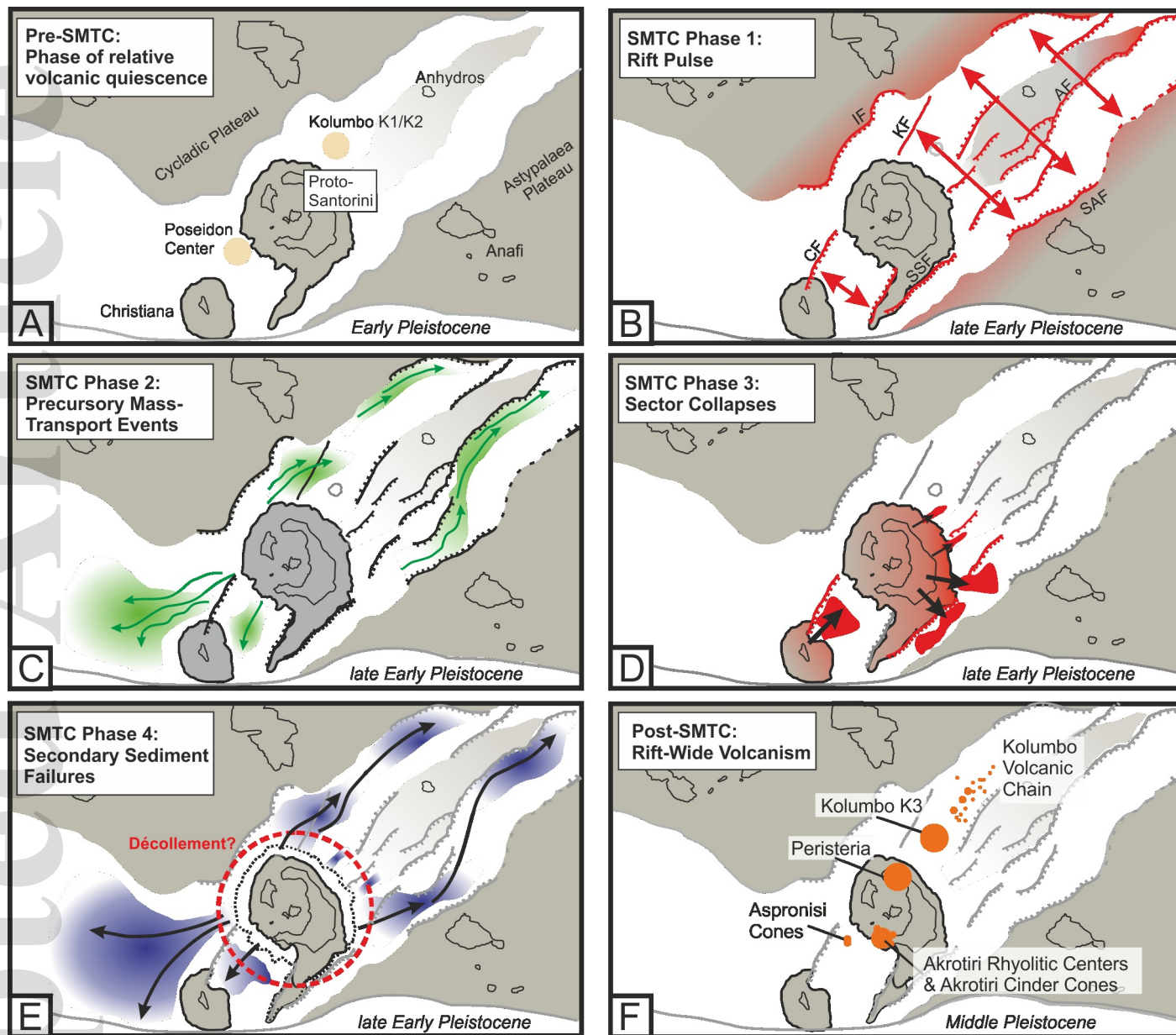bre_12667_f6.png

bre_12667_f7.png

bre_12667_f8.png

bre_12667_f9.png

bre_12667_f10.png

bre_12667_f11_1.png

bre_12667_f11_2.png